2015

The origin of Korotkoff sounds and the accuracy of auscultatory blood pressure measurements

Charles F. Babbs
Purdue University, babbs@purdue.edu

The origin of Korotkoff sounds and the accuracy of auscultatory blood pressure measurements

Charles F. Babbs, MD, PhD*

*Weldon School of Biomedical Engineering, Purdue University, West Lafayette, Indiana, USA

(Journal of the American Society of Hypertension : JASH 2015, 9(12):935-50.e3)

Abstract

This study explores the hypothesis that the sharper, high frequency Korotkoff sounds come from resonant motion of the arterial wall, which begins after the artery transitions from a buckled state to an expanding state. The motion of one mass, two nonlinear springs, and one damper, driven by transmural pressure under the cuff, are used to model and compute the Korotkoff sounds according to principles of classical Newtonian physics. The natural resonance of this spring-mass-damper system provides a concise, yet rigorous, explanation for the origin of Korotkoff sounds. Fundamentally, wall stretching in expansion requires more force than wall bending in buckling. At cuff pressures between systolic and diastolic arterial pressure, audible vibrations (> 40 Hz) occur during early expansion of the artery wall beyond its zero pressure radius after the outward moving mass of tissue experiences sudden deceleration, caused by the discontinuity in stiffness between bucked and expanded states. The idealized spring-mass-damper model faithfully reproduces the time domain waveforms of actual Korotkoff sounds in humans. Appearance of arterial sounds occurs at or just above the level of systolic pressure. Disappearance of arterial sounds occurs at or just above the level of diastolic pressure. Muffling of the sounds is explained by increased resistance of the artery to collapse, caused by downstream venous engorgement. A simple analytical model can define the physical origin of Korotkoff sounds, suggesting improved mechanical or electronic filters for their selective detection, and confirming the disappearance of the Korotkoff sounds as the optimal diastolic endpoint.

Keywords: biomechanics; brachial artery; buckling; diastolic dilemma; muffling; sphygmomanometry.

Introduction

The origin of Korotkoff sounds has remained a subject of debate for over 100 years. These arterial sounds occur during the indirect measurement of blood pressure using an air-filled cuff, usually placed around the upper arm and inflated initially to above the maximal or systolic blood pressure. As cuff pressure is slowly released, arterial sounds can be heard through a stethoscope placed over the artery distal to the cuff or by a microphone placed inside the cuff[1]. Sounds appear as cuff pressure approaches systolic pressure, increase in amplitude, then generally diminish, and finally disappear at a cuff pressure close to the minimal or diastolic blood pressure. Korotkoff himself described three, and later, five phases to the arterial sounds[2-5]: appearance, softening, sharpening, muffling, and disappearance. He speculated that opening and closing of the artery, as net transmural pressure cycled from positive to negative, was responsible for the sounds. This technique has come to be known as the auscultatory method[4, 5]. However, the physical basis of the method remains poorly understood to this day, especially exact biophysical mechanism producing the sounds.

Uncertain also is the temporal relationship of the sounds to true systolic and diastolic pressures. The uncertainty in the end-point for diastolic pressure, in particular, whether it should be taken as the point of muffling or the point of disappearance of the sounds, is known as the diastolic dilemma[3, 6, 7]. The difference between diastolic pressures at muffling and at disappearance of the Korotkoff sounds (as much as 10 mmHg[2, 7]) is clinically significant, because this difference approaches the difference between nominal normal diastolic pressure (80 mmHg) and the threshold for diagnosis and treatment (90 mmHg). Hence the choice of diastolic endpoint can be biologically meaningful and potentially life-changing for patients.

In the absence of a strong theoretical basis for interpreting Korotkoff sounds the clinical community has relied on empirical studies comparing pressures recorded directly with intra-arterial catheters to simultaneous pressures measured by the auscultatory method. A working consensus has evolved that in adults the point of disappearance of arterial sounds is the better indicator of diastolic pressure[2]. However, in children[8], in pregnancy[9], and in exercise[10] there is some evidence that muffling may be a more accurate endpoint. Some authorities recommend recording all three endpoints, for example 120/80/65, to indicate appearance, muffling, and disappearance, although the phenomenon of muffling itself has remained the subject of conjecture rather than biomechanics, and is difficult to define objectively[7].

Accordingly, the objective of the present study was to create and exercise a mathematical model to explore the genesis of Korotkoff sounds and to compute these arterial sounds on the basis of first-principles biomechanics. In particular, the analysis tests the hypothesis that transient resonant vibrations of the arterial wall constitute the underlying mechanism of sound generation. The resulting equations faithfully reproduce the characteristic frequencies and time domain waveforms of the arterial sounds and show that the appearance of the arterial sounds occurs just above the true systolic blood pressure and that the disappearance of the arterial sounds occurs at or just above true diastolic blood pressure. An explanation for the phenomenon of muffling, and simple ways to minimize it, are also presented.

Methods

Approach

Consider a transverse cross section of an artery that is compressed under a blood pressure cuff, as shown in Figure 1. For simplicity, tapering or coning of the vessel in the axial dimension, parallel to the artery[3, 4, 11] is ignored and the forces analyzed are those in the collapsing sub-segment only. To isolate the effects of wall motion, the model also explicitly neglects wave propagation and axial blood flow.

(Please turn to next page.)

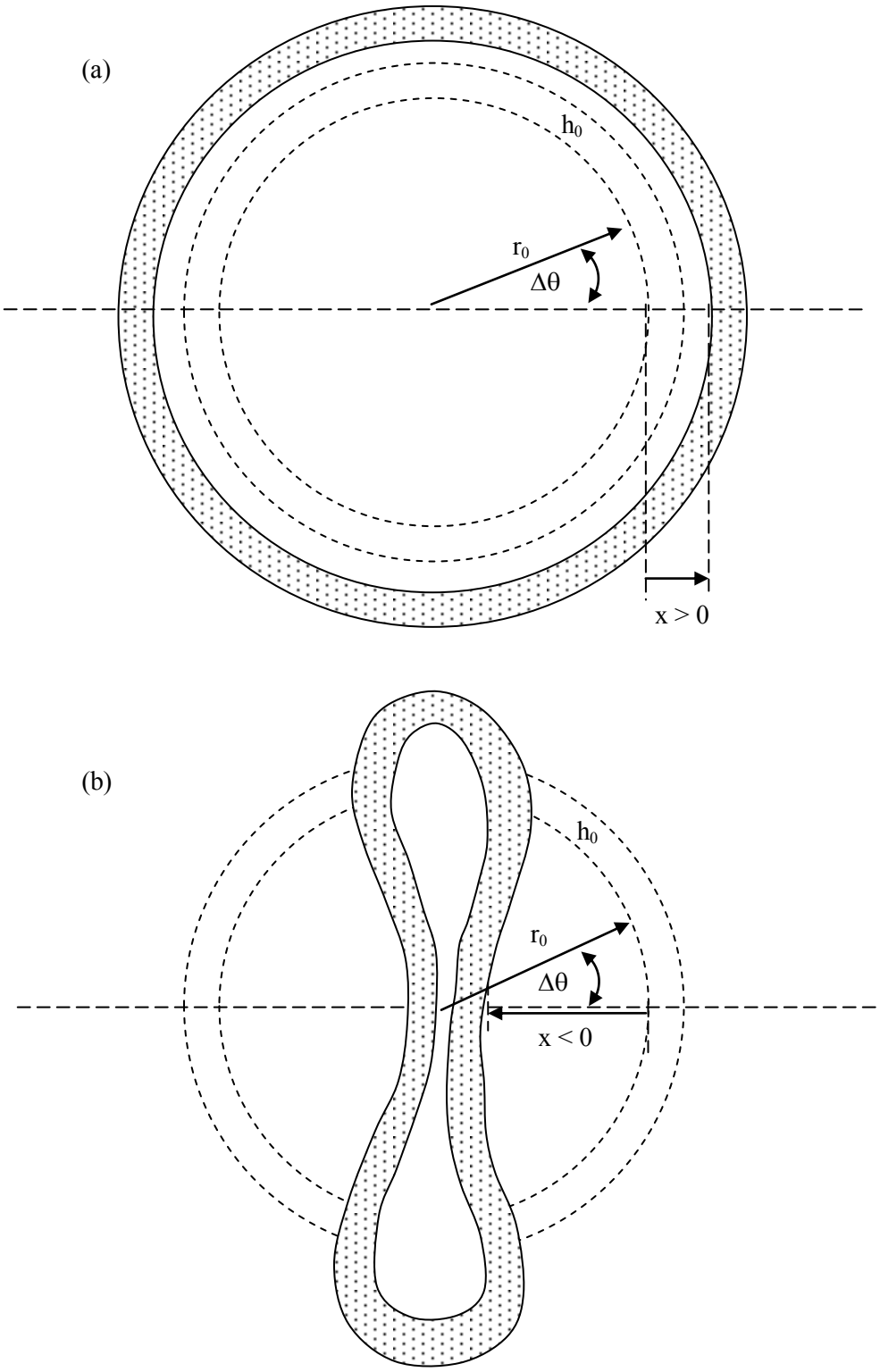

Figure 1. Schematic cross section of an artery in expansion (a) and buckling (b). Shading indicates artery wall. Dotted circles indicate the zero pressure state, and r_0 denotes zero pressure radius. $\Delta\theta$ denotes a specific radial sector. Wall displacement, $x = r - r_0$.

Under positive transmural pressure (inside > outside) expansion of the artery beyond its zero pressure radius, r_0, occurs with radial symmetry. However, under negative transmural pressure (inside < outside) elastic tubes do not shrink with radial symmetry, but rather buckle, when the outside pressure minus the inside pressure, exceeds a threshold buckling pressure[12-15], as shown in Figure 1(b). As the negative transmural pressure increases further, the cross section becomes somewhat elliptical, and then bi-concave or hourglass shaped. Ultimately opposite sides touch at one point and then flatten against one another along a straight-line segment, which increases in length as external pressure increases.

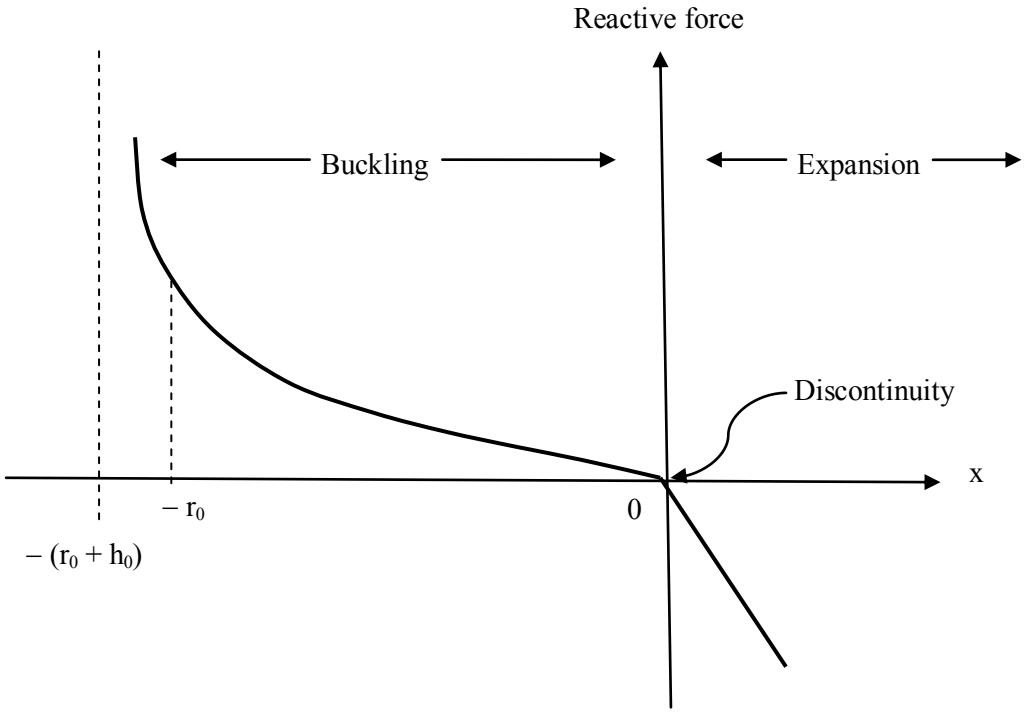

Figure 2. Tube law relating reactive force to change in vessel radius, x, perpendicular to the plane of flattening. During expansion the stretched artery generates inward directed (negative) force. During buckling the compressed artery generates outward directed (positive) force. At the point of buckling there is a sharp discontinuity. In extreme flattening, after opposite walls touch ($x < r_0$), the apparent stiffness of the system in compression, which is related to the slope of the curve, increases to approach, and ultimately exceed, the stiffness of the tube in radial expansion.

Unlike expansion, buckling occurs rapidly with modest negative transmural pressures[11, 13, 16]. This phenomenon means that the slope of the pressure-area curve, which is related to vessel stiffness, abruptly changes at the collapse pressure. The collapse pressure is equal to, or slightly less than zero (Figure 2). Vessel compliance is greatest when the transmural pressure is moderately negative. Importantly in the present context, there is a large discontinuity in the

value of the compliance at the collapse pressure[12-14]. Bertram[12], for example, studied pressure-area curves in silicone rubber tubing, finding that the compliance was one to two orders of magnitude greater during bucking than during distension (and stiffness one to two orders of magnitude less). The obvious differences in the magnitudes of the forces involved in stretching and buckling can be appreciated by any reader using an ordinary rubber band. The hypothesis underlying the present work is that the discontinuity at the point of buckling[12-15, 17, 18] is key to production of Korotkoff sounds. In particular, transient harmonic oscillation in artery wall position, or ringing, occurs just after the expanding artery transitions from the buckled state to the radially expanded state. This state transition causes a sudden deceleration of wall motion, which produces ringing.

One dimensional model

Let x represent the displacement of the inner wall of the artery from its zero pressure equilibrium radius, r_0, in a direction perpendicular to the plane of flattening, as shown in Figure 1. Let $x^* = -\varepsilon r_0$ for $0 \le \varepsilon << 1$ be the point in the x-domain at which buckling begins. During expansion x is greater than zero, and the outward motion of the wall and surrounding fluid is symmetrically radial. During buckling x is less than $-\varepsilon r_0$, and there is collapse with ultimate flattening. For purposes of the present model, the inward motion of the majority of surrounding fluid mass during buckling phase is regarded as approximately radial, as sketched in Figure 3(a). This insight leads to an equivalent one dimensional motion problem, in which the time domain waveform x(t) essentially describes artery wall motion. The fat and loose connective tissues surrounding the artery are represented by mass only, without significant elasticity.

Thus the physics of arterial wall motion under the cuff can be modeled in one dimension, as shown in Figure 3(b). A mass, m, representing the effective mass of a given length of artery and surrounding fluid, as specified subsequently, is constrained by two nonlinear springs. Spring k_1 represents the reactive elastic force resisting expansion under positive transmural pressure for $x > x^* = -\varepsilon r_0$. This inward directed force, $-k_1 x$, is produced by circumferential elastic fibers and collagen in the artery wall. Spring k_2 represents the reactive elastic force resisting collapse under negative transmural pressure with buckling when $x < x^* = -\varepsilon r_0$. This outward directed force, $-k_2 x > 0$, is produced by bending of the artery wall.

Only one of the two springs in Figure 3 is compressed at any one time, as indicated by the bumpers at the far right and far left. At the zero pressure equilibrium point ($x = 0$) neither spring is compressed, and the reactive force is zero. Both k_1 and k_2 are in general non-linear; although during expansion k_1 can be regarded as constant for simplicity. During early buckling the elastic force, $-k_2 x$, is weak compared to a comparable amount of expansion. The nonlinear property of k_2 begins to dominate as x becomes more negative and approaches $-r_0$, owing to the more complex bending producing the hourglass shaped cross section. Then, as x approaches $-(r_0 + h_0)$, the value of k_2 approaches infinity, owing to the boundary condition enforced by the plane of symmetry. In this regime the gradual, rather than abrupt, increase in k_2 tends to cushion sudden deceleration of the artery wall.

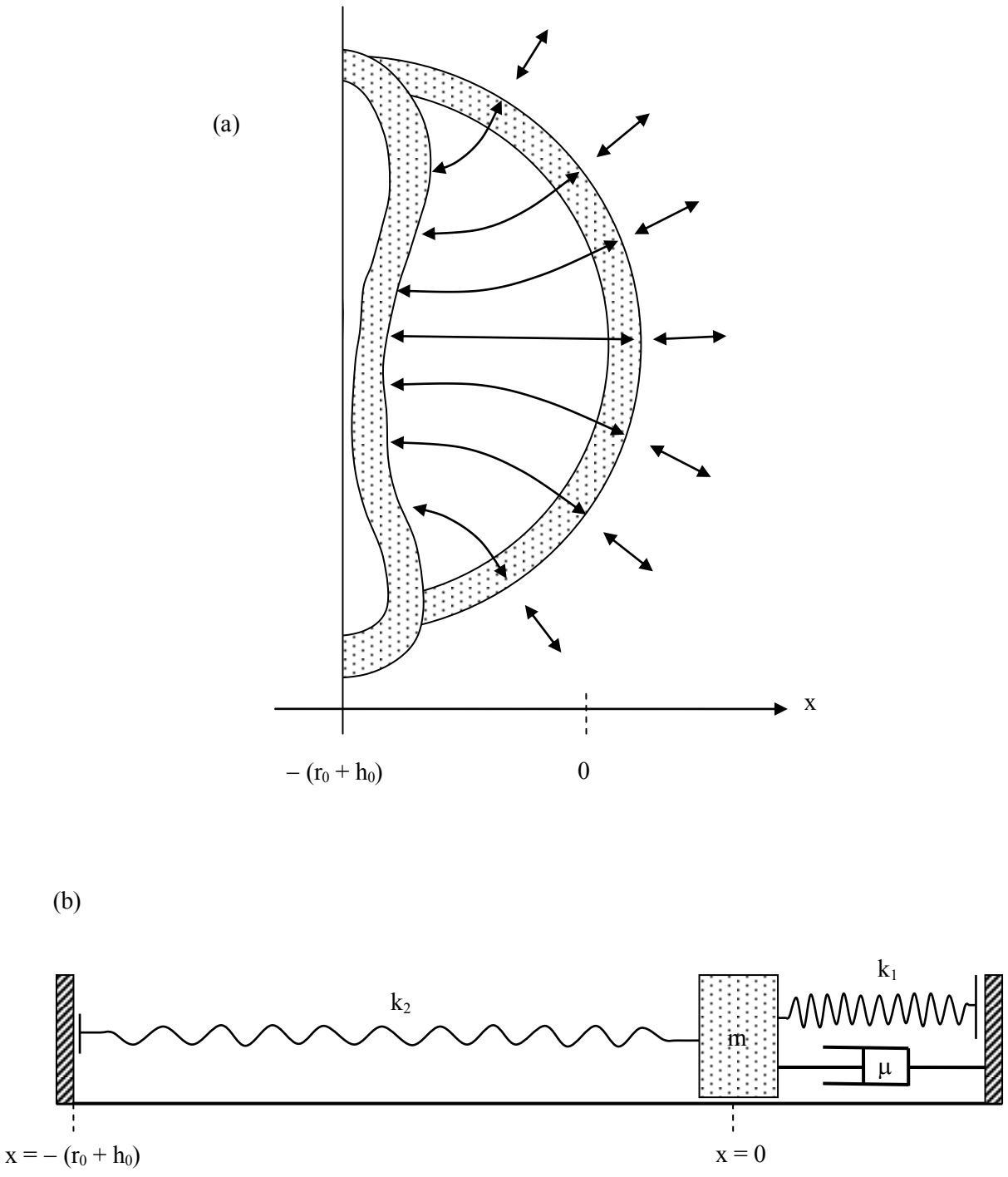

Figure 3. Equivalent spring-mass-damper system for pulsating artery under a blood pressure cuff. (a) Generally radial motion of fluid mass. (b) Nonlinear springs for expansion, k_1, and buckling, k_2, and damper, μ.

Elastic forces in expansion

As shown in Appendix 1 the spring constant, k_1, for small positive displacements is given from first principles of physics as

$$k_1 \approx EL\frac{h_0}{r_0}\Delta\theta, \tag{1}$$

where E is Young's modulus of elasticity of the artery wall, L is axial length of the segment, h_0 is the zero pressure wall thickness, r_0 is the zero pressure internal radius of the artery, and $\Delta\theta$ is the angular sector of artery wall, as shown in Figure 1. As the artery stretches slightly, E increases, owing to the nonlinear elastic properties of biomaterials, and h/r decreases by geometry and by conservation of wall volume, so for modest distensions of the artery under the relatively small transmural pressures during cuff deflation, k_1 can be taken as a constant. The reactive force in Figure 2 is $F(x) = -k_1 x$ for $x > x^*$.

Elastic forces in buckling

In general, the variable spring coefficient, k_2, can be regarded as the total reactive force in the x-dimension during buckling, divided by the compressed distance, $|x|$. This "spring back" force increases nonlinearly as x becomes increasingly negative. The total force resisting flattening can be modeled by a curvilinear function with positive constants a and b of the form

$$F(x) = -\frac{ax}{b+x}, \text{ for } x \le x^*. \tag{2}$$

In turn,

$$k_2(x) = \frac{F(x)}{|x|} = \frac{a}{b+x}. \tag{3}$$

By inspection, b must equal $(r_0 + h_0)$, the ultimate physically possible degree of flattening, so that as $x \to -(r_0 + h_0)$, $F(x) \to \infty$. As shown in Appendix 2, based on elementary mechanics, $k_2(-r_0) \approx 4\frac{EL}{\pi^2}\cdot\frac{h_0^2}{r_0^2}\Delta\theta$. For the nonlinear spring model we have, for $x = -r_0$

$$k_2(-r_0) = 4\frac{EL}{\pi^2}\cdot\frac{h_0^2}{r_0^2}\Delta\theta = \frac{a}{b-r_0} = \frac{a}{h_0}, \tag{4}$$

giving a useful expression for constant, a, namely

$$a = 4\frac{EL}{\pi^2}\cdot\frac{h_0^3}{r_0^2}\Delta\theta. \tag{5}$$

Then using (2) in (5), with $b = r_0 + h_0$,

$$k_2(x) = 4\frac{EL}{\pi^2}\cdot\frac{h_0^2}{r_0^2}\cdot\frac{h_0}{r_0 + h_0 + x}\Delta\theta, \quad \text{for } x < x^*. \tag{6}$$

Equation (6) gives a formula for spring coefficient, $k_2(x)$, in terms of basic model parameters.

In relative terms for $k_1 = EL\frac{h_0}{r_0}\Delta\theta$, the ratio

$$\frac{k_2(x)}{k_1} = \frac{4}{\pi^2}\cdot\frac{h_0}{r_0}\cdot\frac{h_0}{r_0 + h_0 + x}. \tag{7}$$

Hence for x near zero, the local spring constant for buckling is substantially less than that for expansion. For example, if $h_0/r_0 = 1/3$ and $x^* = 0$, then $k_2(0)/k_1 = 0.101$. The artery is 10 times stiffer in expansion than in buckling, with a sharp discontinuity at x^*. As displacement x becomes progressively more negative, indicating a greater degree of flattening, $k_2(x)$ gradually increases to a value $\frac{4}{\pi^2}\cdot\frac{h_0}{r_0}$, or about 13% of k_1 when $x = -r_0$, and then rapidly increases with further flattening. Thus, in a fundamental sense wall bending in buckling requires much less force than wall stretching in expansion. Hence, $k_2(x)/k_1(x) << 1$ for small values of x is an expected and constant feature of collapsible elastic tubes, such as arteries.

Effective mass

As shown in Appendix 3 the effective mass of the tissue that is accelerated by radial motion of the arterial wall is a function of the tissue mass density, ρ, the axial length, L, the zero pressure radius, r_0, and the mean radius of tissue surrounding the artery, R_{max}, so that in this model of cylindrical symmetry

$$m \approx \Delta\theta\rho L r_0 R_{max}. \tag{8}$$

Damping

The lumped energy loss due to viscous damping in the system is represented by a single dashpot shown in Figure 3. The value of the damping modulus, D, can be estimated from measured

viscoelastic properties of arterial wall during expansion at the frequencies of Korotkoff sounds. In turn, by analogy with Equation (1) the lumped damping constant, μ, can be expressed as

$$\mu = DL\frac{h_0}{r_0}\Delta\theta\,. \tag{9}$$

Driving force

Regarding the artery as a relatively thin walled cylinder, the driving force for motion of the arterial wall is provided by the difference between internal pressure, P_i, and external pressure, P_o, on the artery wall, multiplied by the surface area over which the pressure acts. Both in limited radial expansion and in buckling the relevant surface area for a particular sector, $\Delta\theta$, of the artery wall is $Lr_0\Delta\theta$. In turn, the driving force becomes

$$F(x,t) = \left(P_i(t) - P_o(t)\right)\cdot Lr_0\Delta\theta\,. \tag{10}$$

Equation of motion for the system

Combining the forgoing parts from Equations (1), (6), (8), and (9), using Newton's second law of motion (net force = mass x acceleration) with "dot" and "double dot" notation for the first and second time derivatives ($\dot{x} = dx/dt$, $\ddot{x} = d^2x/dt^2$), we have after cancelling the $L\Delta\theta$ terms, the following equations of motion for the arterial wall:

$$\left(P_i(t) - P_o(t)\right)\cdot r_0 - E\frac{h_0}{r_0}x - D\frac{h_0}{r_0}\dot{x} = \rho r_0 R_{max}\ddot{x} \quad \text{for } x > x^* \tag{11a}$$

$$\left(P_i(t) - P_o(t)\right)\cdot r_0 - 4\frac{E}{\pi^2}\cdot\frac{h_0^2}{r_0^2}\cdot\frac{h_0}{r_0 + h_0 + x}x - D\frac{h_0}{r_0}\dot{x} = \rho r_0 R_{max}\ddot{x} \quad \text{for } x \le x^*. \tag{11b}$$

These equations can be solved for wall displacement, x, as a function of time to characterize any arterial wall vibrations, or lack thereof, during cuff deflation.

Numerical values of model parameters

Arteries are composite materials, and the more they are stretched the stiffer they become, owing to the recruitment of collagen fibers and uncoiling of elastic fibers in the arterial wall. Hence Young's elastic modulus, E, for arteries is nonlinearly dependent on the distending pressure[4, 19]. In the context of the present problem what is needed is a numerical value for Young's modulus of arteries experiencing transmural pressures during cuff deflation ranging from – 40 to + 40 mmHg in individuals with normal blood pressure. Bank[20], for example, found for human

brachial arteries in vivo that Young's modulus at normal arterial pressures is about four times greater than that at lower pressures of cuff deflation (0 to 40 mmHg). Similarly, Holzapfel and Ogden[18] showed theoretically that Young's modulus at normal arterial pressure is about four times greater than Young's modulus in the range of 0 to 40 mmHg. However, most experimental data are obtained at normal arterial pressures. Cox[21] summarized measured elastic moduli at mean arterial pressures near 140 mmHg ranging from 1 to 4 x 10^6 dynes/cm^2. Taking one quarter of these values would translate to 0.25 to 1 x 10^6 dynes/cm^2 transmural pressure during cuff deflation. Gow[22] in living dogs found arterial elastic moduli ranging from 0.4 to 8 and averaging about 2 x 10^6 dynes/cm^2, which would translate to 0.1 to 2 x 10^6 dynes/cm^2 during cuff deflation. Young's modulus is given directly for pressures ranging from 20 to 40 mmHg in Bergel's thesis[23] (Figure 14, p. 123) and averages 2 x 10^6 dynes/cm^2. Bank[20], using ultrasound measurements in living human subjects found values of E ranging from 0.5 to 5 x 10^6 dynes/cm^2 and averaging about 2 x 10^6 dynes/cm^2 in the pressure range of 0 to 40 mmHg. In aggregate these data suggest a working value for E near 1.4 x 10^6 dynes/cm^2 for the low transmural pressures operative during cuff deflation.

In assigning a numerical value for the damping modulus, D, of the arterial wall it is important to realize that arterial wall viscosity is highly frequency dependent. If one regards the arterial wall as being represented by a simple Kelvin-Voigt element consisting of a spring and dashpot in parallel, then the viscous constant for the dashpot can be determined from experimental data. The classic study of Lawton[24] on isolated aortic strips of the dog found a hyperbolic relation between frequency and the ratio of damping modulus to elastic modulus (D/E). Extrapolating this hyperbolic relationship to the frequency range of Korotkoff sounds near 60Hz with E = 1.4 x 10^6 dynes/cm^2 gives the value 286 dyne-sec/cm^2 for D. The data of Gow and Taylor[22] reveal a damping modulus of about 1300 dyne-sec/cm^2 at 60 Hz. The synthetic model of Cox[21] (Figure 6 in Cox) used to fit the experimental data of Bergel predicts that the value of the elastic modulus levels out at about 400 dyne-sec/cm^2 at angular frequencies over 100 radians/sec. A similar analysis of the data of Learoyd[25] gives a damping modulus of 845 dyne-sec/cm^2 at 60 Hz natural frequency. Averaging these estimates gives a damping modulus for the standard arterial model of 708 dyne-sec/cm^2 at the frequency of Korotkoff sounds.

Zero pressure wall radius is 1.5 mm or 0.l5 cm according to Bank[20]. Learoyd and Taylor[25] give wall thickness ratio h/r of about 0.15 at low pressures < 50 mmHg, so that the wall thickness would be 0.225 mm or 0.022 cm. Betik et al.[26] found in control subjects using ultrasound at normal arterial pressures brachial artery radii averaging 0.22 cm. Iwamoto et al.[27], using ultrasound in adult human subjects with normal blood pressure found brachial artery radius averaging 0.2 cm and wall thickness 0.03 cm. Weidinger[28] in patients without coronary artery disease found brachial artery wall thickness averaging 0.035 cm, and Suessenbacher[29] found 0.037 cm value in a similar study. Aggregating these data gives a working estimate of zero pressure artery radius, r_0, of 0.2 cm and zero pressure wall thickness, h_0, of 0.03 cm for the human brachial artery.

Tissue density is taken as 1.0 g/cm^3, that of water. The average radius of the arm, R_{max}, is taken as 5 cm, according to Wijnhoven[30], and used as a measure of the typical artery to skin surface distance, here ignoring any effects of bone for the sake of simplicity.

Table 1 lists numerical values of standard model parameters obtained from the literature. There are no free or fitted parameters, except for ε. For initial simulation it was assumed that buckling begins at $x = 0$, and $r = r_0$, so that $\varepsilon = 0$ and $x^* = 0$. In later simulations the consequences of bucking happening at increasingly more negative fractions of the zero pressure radius were explored, with $\varepsilon = 0.01$ to 0.04, and $x^* = -0.01r_0$ to $-0.04r_0$.

Table 1: Model Parameters

Symbol	Variable description	Standard value	Units	References
E	Elastic (Young's) modulus	1.4×10^6	dyne/cm^2	Bank[20], Cox[21], Gow[22], Holzapfel[18], Bergel[23]
D	Damping modulus	738	dyne-sec/cm^2	Lawton[24], Gow[22], Cox[21], Learoyd[25]
r_0	Zero pressure internal radius	0.2	cm	Bank[20], Betik[11], Iwamoto[31])
h_0	Zero pressure wall thickness	0.03	cm	Learoyd[25], Iwamoto[27], Weidinger[28])
P_i	Internal artery pressure	80 – 120	mmHg	Boron[32]
P_o	External artery (cuff) pressure	60 – 130	mmHg	Geddes[4]
R_{max}	Average adult human arm radius	5	cm	Wijnhoven[30]
ε	Fraction of zero pressure radius where buckling begins	0 – 0.04		

Simulated blood pressure waveform

To initiate wall motion, internal artery pressure $P_i(t)$ was simulated using a simplified Fourier series to approximate the arterial pulse waveform as a function of time, t, as described by Geddes and Baker[33]:

$$P_i(t) = DBP + 0.5 \cdot PP + 0.36 \cdot PP \cdot \left[\sin(\omega t) + \frac{1}{2}\sin(2\omega t) + \frac{1}{4}\sin(3\omega t) \right], \qquad (12)$$

where DBP is diastolic blood pressure (normally 80 mmHg), PP (normally 40 mmHg) is pulse pressure (systolic minus diastolic), and ω is the angular frequency of the heart beat, that is, $\omega = 2\pi f$ for cardiac frequency, f, in Hz.

External artery or cuff pressure was taken as a linear ramp from 130 mmHg at the beginning of a blood pressure determination to 70 mmHg at the end of the run for the normal pressure case, namely, SBP/DBP = 120/80 mmHg. The cuff deflation rate was 3 mmHg/sec, and the pulse frequency was one per second. In some simulations cuff pressure was held constant to examine details of simulated arterial sound waveforms.

Numerical methods

Equations (11) were solved numerically as follows, beginning with suitable initial conditions. Acceleration was computed from the governing equations as

$$\ddot{x} = \frac{1}{\rho r_0 R_{max}} \left[\left(P_i(t) - P_o(t)\right) \cdot r_0 - E\frac{h_0}{r_0}x - D\frac{h_0}{r_0}\dot{x} \right] \quad \text{for } x > x^* \qquad (13a)$$

and

$$\ddot{x} = \frac{1}{\rho r_0 R_{max}} \left[\left(P_i(t) - P_o(t)\right) \cdot r_0 - 4\frac{E}{\pi^2} \cdot \frac{h_0^2}{r_0^2} \cdot \frac{h_0}{r_0 + h_0 + x}x - D\frac{h_0}{r_0}\dot{x} \right] \quad \text{for } x \le x^*. \qquad (13b)$$

Then for successive small time steps $\Delta t = 0.01$ msec the simple Euler method was implemented to create marching solution: $\dot{x} \leftarrow \dot{x} + \ddot{x}\Delta t$ and $x \leftarrow x + \dot{x}\,\Delta t$. The raw output of the model equations is a record of wall velocity, $\dot{x}$, and wall displacement, x, as a function of time, t.

To simulate sonic waves caused by compression and rarefaction of molecules, the time derivative of wall displacement, $\dot{x}$, was used as a surrogate for sound pressure level and tabulated each millisecond . To simulate the frequency response of a stethoscope in the range of 20 to 100 Hz[17], the wall velocity data were high pass filtered such that frequencies below 20 Hz

were attenuated by 90 percent and frequencies above 100 Hz were attenuated between zero and five percent.

Results

Arterial sounds and the diastolic endpoint

Figure 4 shows the result of a simulated blood pressure determination with linear cuff deflation from 10 mmHg above normal systolic pressure to 10 mmHg below normal diastolic pressure. The time base is condensed to 20 sec to show the complete event. The top record (a) shows arterial pressure and cuff pressures. The second record (b) shows raw arterial wall velocity (dx/dt), and the third (c) shows high pass filtered arterial wall velocity (filtered dx/dt) as a surrogate for sound entering the ear canals of the examiner. The bottom record (d) shows arterial wall position, x, as a function of time. As the cuff is deflated below systolic pressure, the arterial wall begins to expand and collapse in response to the cycling of transmural pressure from positive to negative. Higher frequency vibrations, the arterial sounds, appear near systolic pressure and cease near diastolic pressure. The envelope of the simulated arterial sounds on the compressed time scale is similar to that of classically recorded Korotkoff sounds[34]. The quality and nature of the high pass filtered sounds change over the course of the cuff deflation run, with some of the beats having a double or split sound and some of the beats having a single sound. After 16 seconds, when wall position no longer cycles into negative territory, the arterial sounds cease.

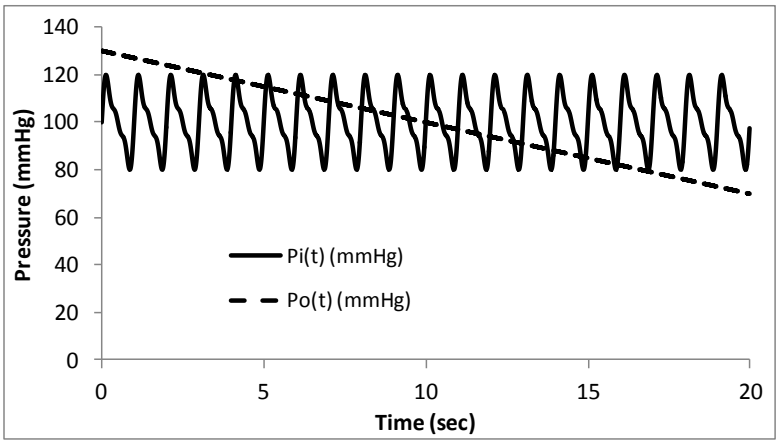
Pressure (mmHg)
Time (sec)
Pi(t) (mmHg)
Po(t) (mmHg)
0
20
40
60
80
100
120
140
0
5
10
15
20

(a)

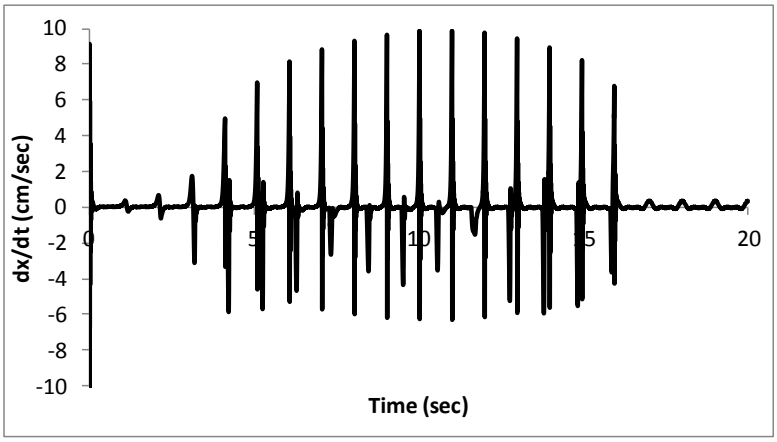
dx/dt (cm/sec)
Time (sec)
10
8
6
4
2
0
-2
-4
-6
-8
-10
0
5
10
15
20

(b)

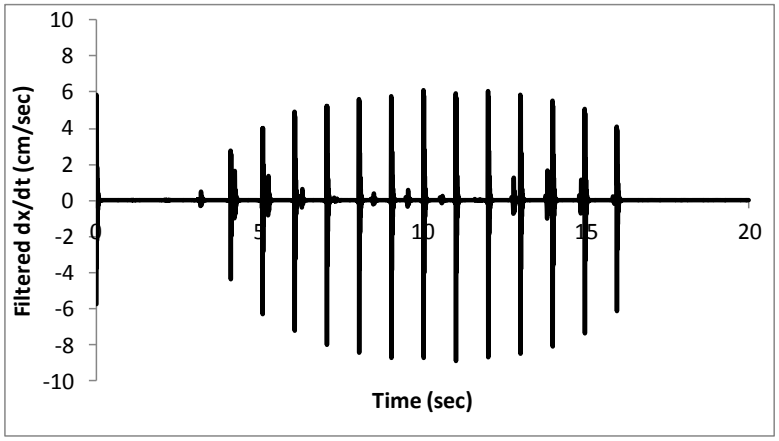
Filtered dx/dt (cm/sec)
Time (sec)
10
8
6
4
2
0
-2
-4
-6
-8
-10
0
5
10
15
20

(c)

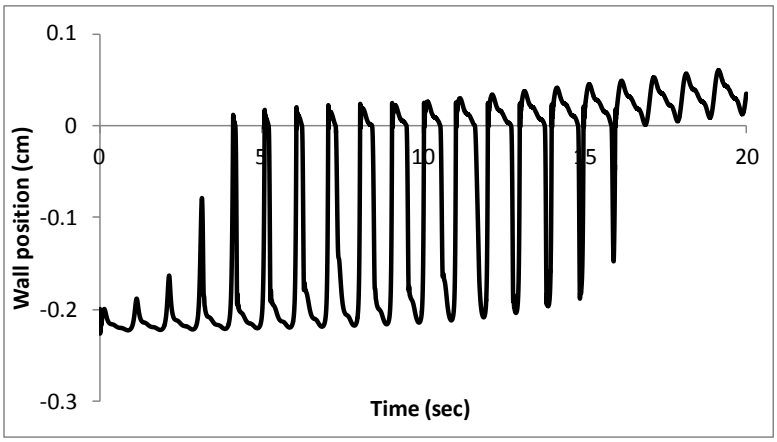

(d)

Figure 4. Simulated auscultatory blood pressure measurement with the standard model. (a) Arterial pulses, $P_i(t)$, and cuff pressure, $P_o(t)$ in the time domain. (b) Raw arterial wall velocity (dx/dt) as a surrogate for sound pressure. (c) High pass filtered wall velocity (filtered dx/dt) simulating sound heard at end of stethoscope. (d) Absolute wall position, x, as a function of time.

Arterial wall vibrations are better appreciated by examining single beats at a specific, constant cuff pressure on an expanded time scale. Figure 5 shows the sound (filtered dx/dt) and arterial wall motion channels for cuff pressure at 122 mmHg, just slightly above the systolic intra-arterial pressure of 120 mmHg. The arterial pressure approaches cuff pressure, and the transmural pressure approaches, but does not reach, zero. In turn, the wall position changes from a maximally flattened state to a nearly half open state. Thereafter, as transmural pressure returns toward the maximal negative value, there is a deceleration with slight ringing in the motion of the effective mass moved by the pulsating artery. This collapse phase ringing is accentuated at a cuff pressure equal to systolic pressure (Figure 6).

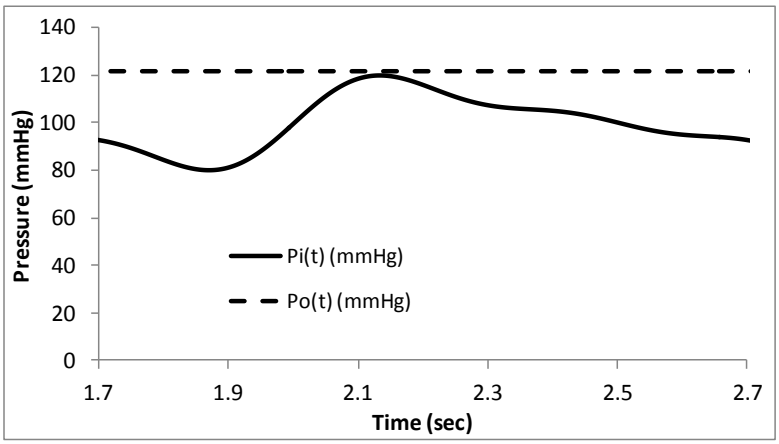

(a)

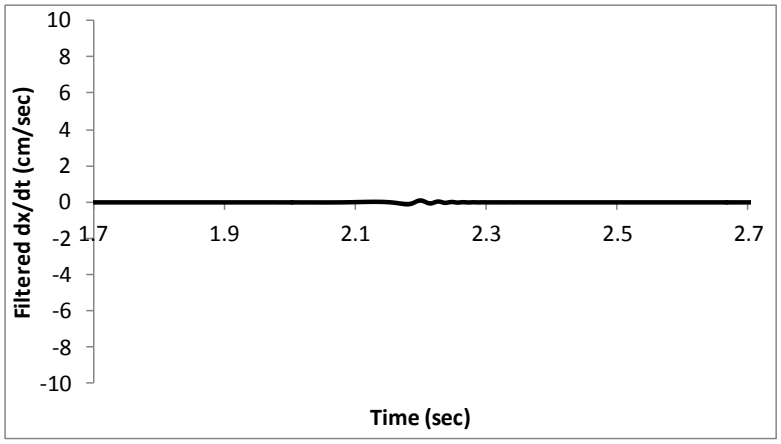

(b)

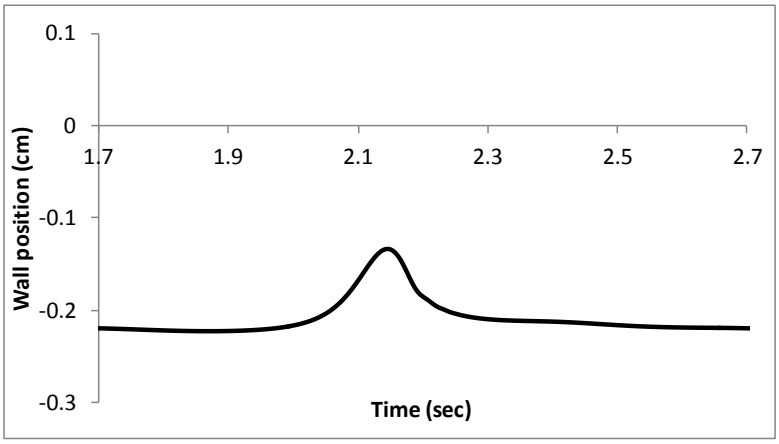

(c)

Figure 5. Simulated wall motion on an expanded time scale with cuff pressure slightly above true systolic pressure. (a) Arterial pulses, $P_i(t)$, and cuff pressure, $P_o(t)$ in the time domain. (b) High pass filtered wall velocity (filtered dx/dt) showing faint sonic vibrations as wall returns to flattened state. (c) Absolute wall position, x, as a function of time.

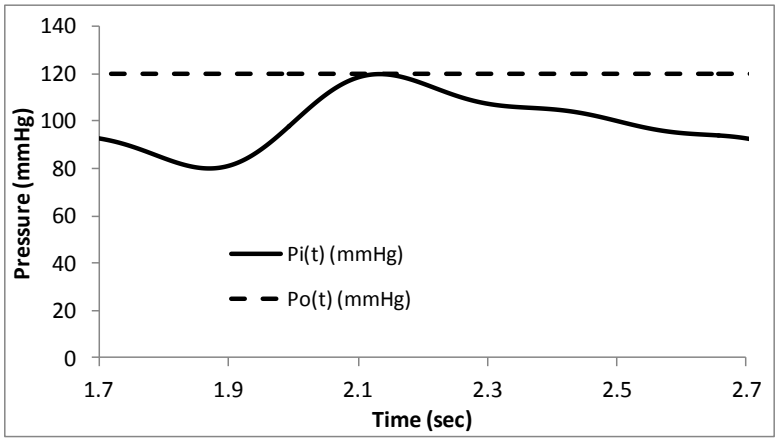

(a)

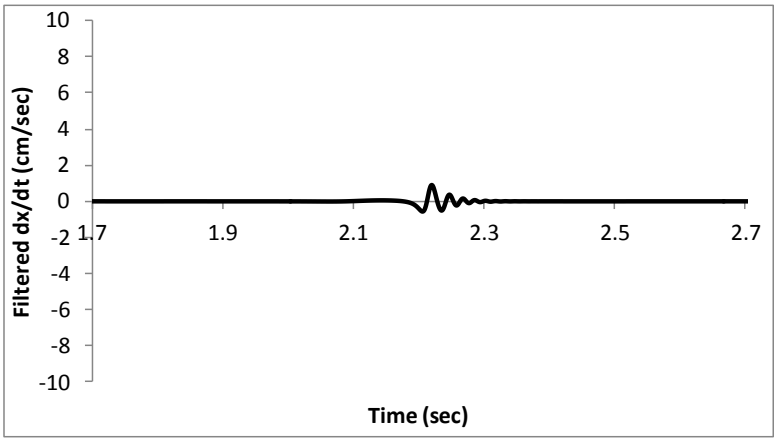

(b)

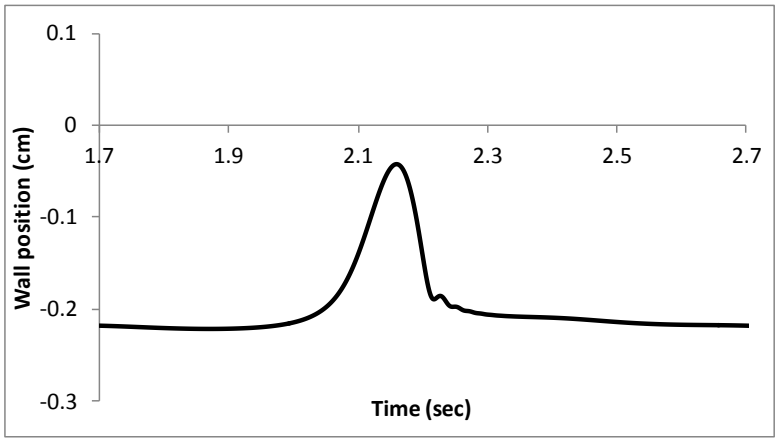

(c)

Figure 6. Simulated wall motion with cuff pressure equal to true systolic pressure. Details similar to Figure 5. Middle plot (b) shows audible sounds (filtered dx/dt). Collapse to a flattened state near time 2.2 sec produces a transient, low amplitude sound.

When transmural pressure becomes briefly positive at cuff pressure 118 mmHg, a new pattern of wall vibration is seen (Figure 7), with resonance occurring first at the upstroke of the arterial pulse, as wall position crosses briefly from the collapsed state to the expanded state. This resonance leads the previously described collapse phase resonance in time, and causes a splitting of the arterial sound. At 115 mmHg cuff pressure (Figure 8) the expanded state lasts much longer than the collapsed state, and the expanded state resonance is more prominent and higher in frequency than the collapsed state resonance. Sonic frequencies are evident in the wall motion tracings, especially after the wall displacement transitions from negative to positive. The analytically calculated resonant frequency of the artery wall in the expanded state is 72 Hz. The numerically calculated resonant frequency of the artery wall in the expanded state is near 75 Hz.

(Please turn to next page.)

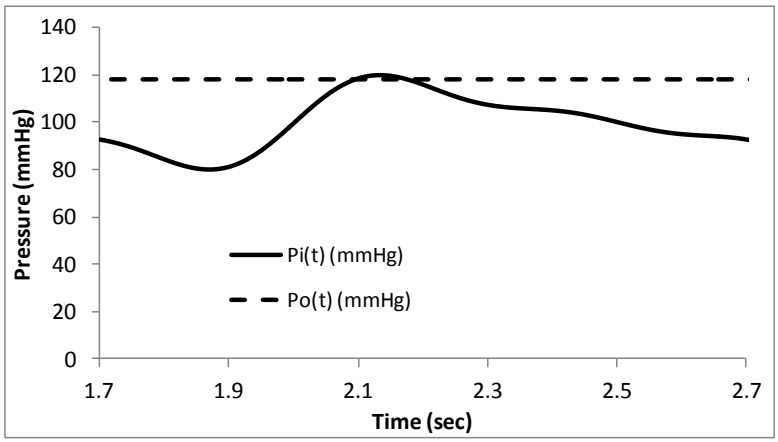

(a)

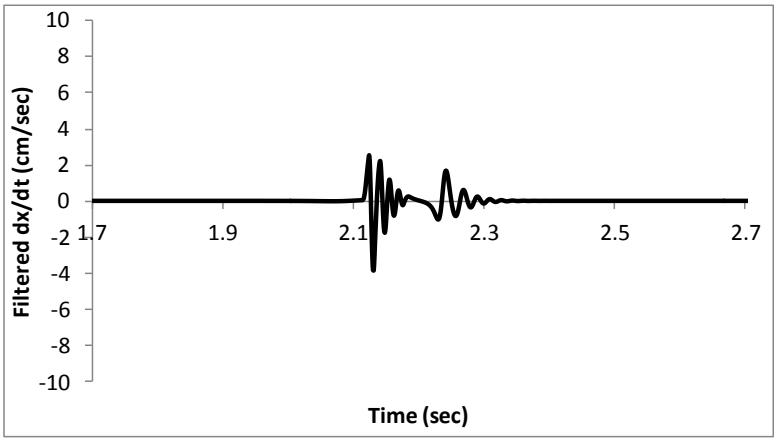

(b)

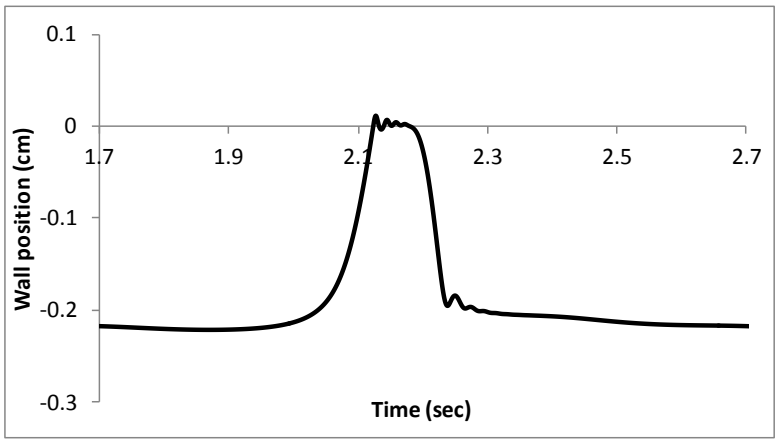

(c)

Figure 7. Simulated wall motion with cuff pressure at 118 mmHg, 2 mmHg below true systolic pressure. Details similar to Figure 5. Middle plot (b) shows audible sounds (filtered dx/dt). Both expansion and collapse produce transient, low amplitude sounds. The expansion phase sound has higher frequency, associated with the larger effective spring constant of the expanded arterial wall.

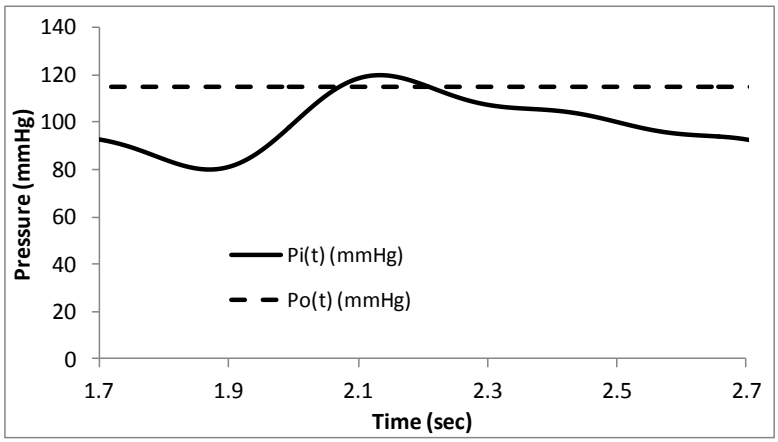

(a)

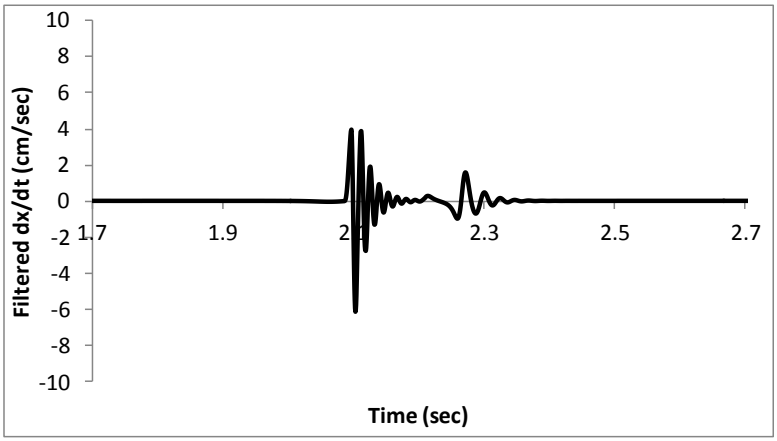

(b)

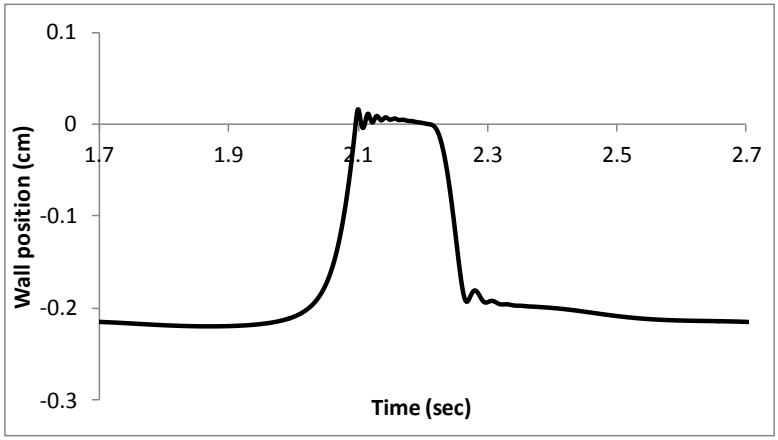

(c)

Figure 8. Simulated wall motion with cuff pressure at 115 mmHg. Middle plot (b) shows audible sounds (filtered dx/dt). Details similar to Figure 5.

At 100 mmHg near mean aortic pressure (Figure 9) the expanded state resonance dominates the sound channel and the collapsed state resonance is greatly attenuated. This trend continues as cuff pressure is further reduced. At 85 and 82 mmHg cuff pressures, which are just above true diastolic blood pressure (Figures 10 and 11) sonic frequencies of wall oscillation occur almost exclusively just after transition from the collapsed to the expanded state. In general, the expanded state resonances dominate, with changes in amplitude and subtle changes in frequency. The collapsed state resonances occur at somewhat lower frequencies than the expanded state resonances. These simulations show that wall vibrations can produce sounds in the audible frequency range > 20 Hz.

(Please turn to next page.)

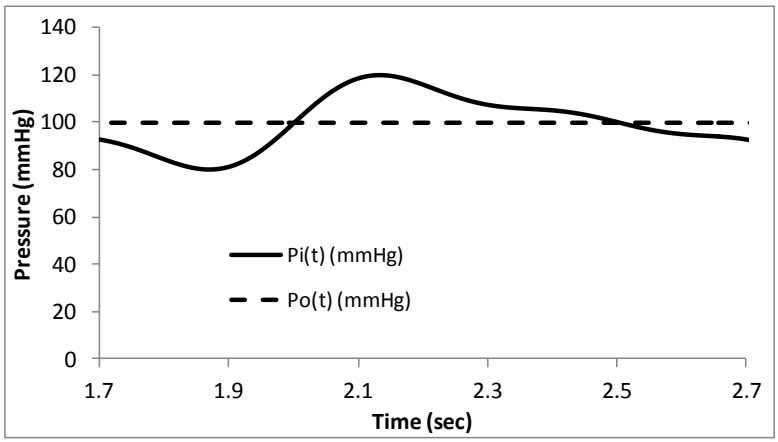

(a)

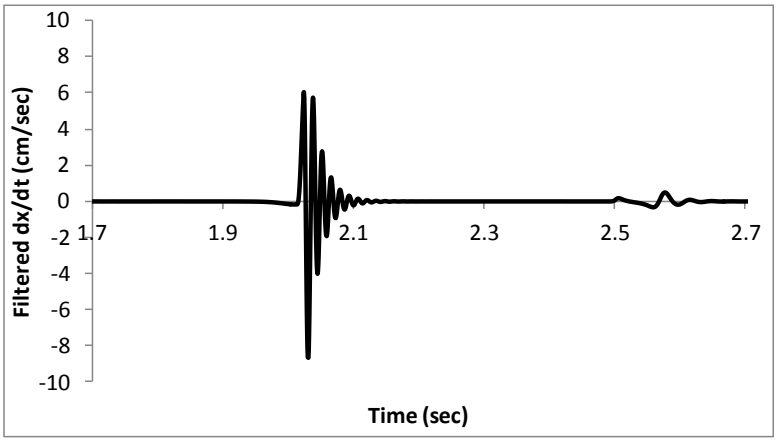

(b)

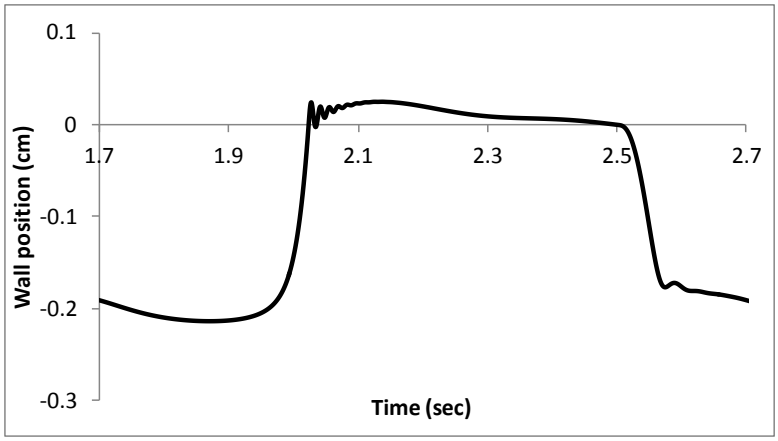

(c)

Figure 9. Simulated wall motion with cuff pressure at 100 mmHg. Middle plot (b) shows audible sounds (filtered dx/dt). Details similar to Figure 5.

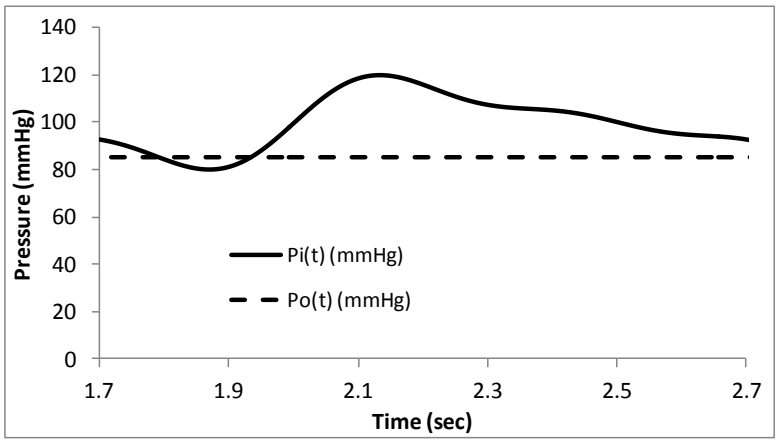

(a)

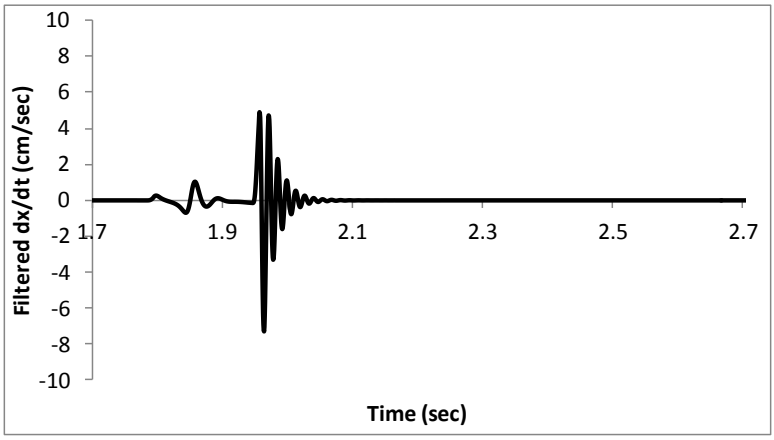

(b)

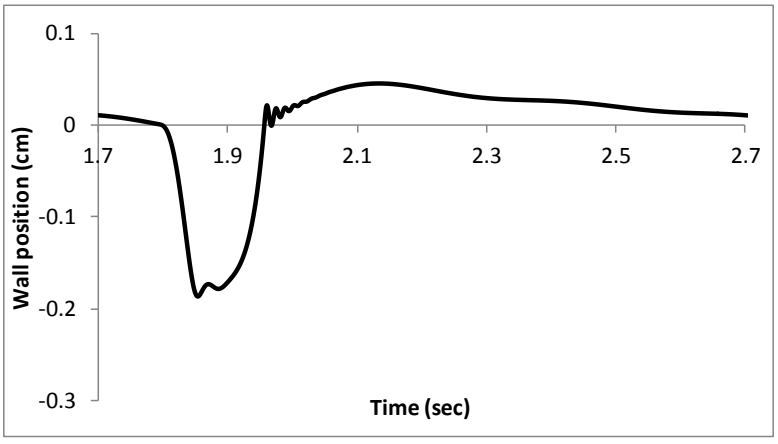

(c)

Figure 10. Simulated wall motion with cuff pressure at 85 mmHg. Middle plot (b) shows audible sounds (filtered dx/dt). Details similar to Figure 5.

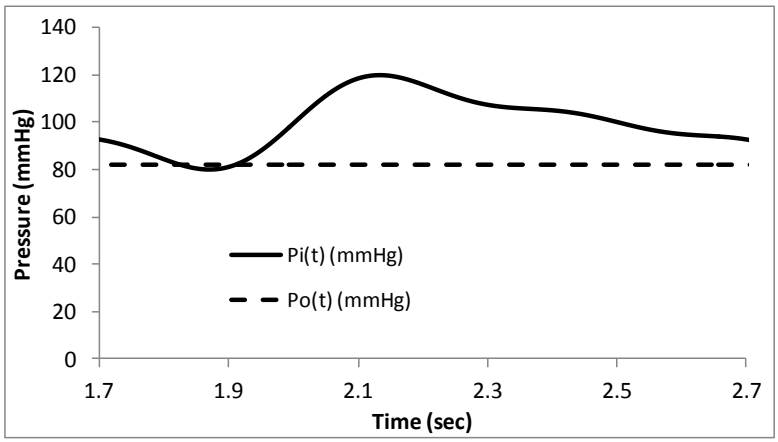

(a)

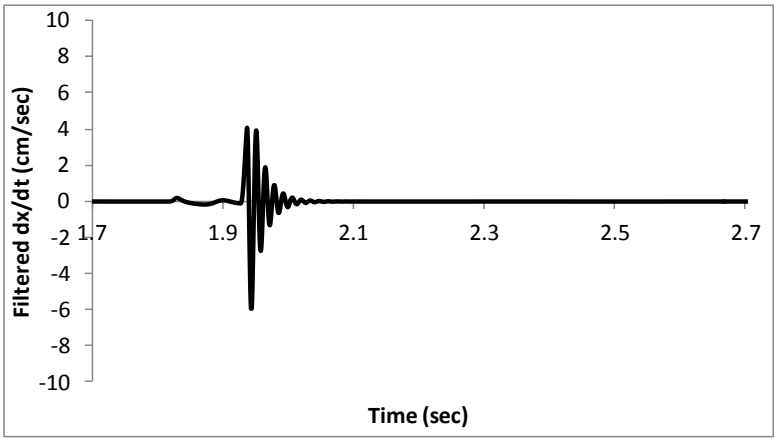

(b)

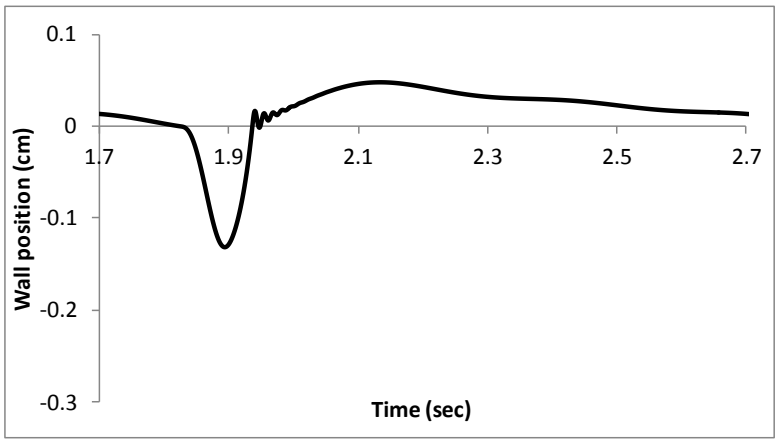

(c)

Figure 11. Simulated wall motion with cuff pressure at 82 mmHg. Middle plot (b) shows audible sounds (filtered dx/dt). Details similar to Figure 5.

Interestingly as shown in Figure 12, at a cuff pressure exactly equal to true diastolic pressure (80 mmHg), the sounds disappear. The artery is always distended and in the regime of expansion.

This result supports the choice of the disappearance of arterial sounds as the correct endpoint for diastolic pressure.

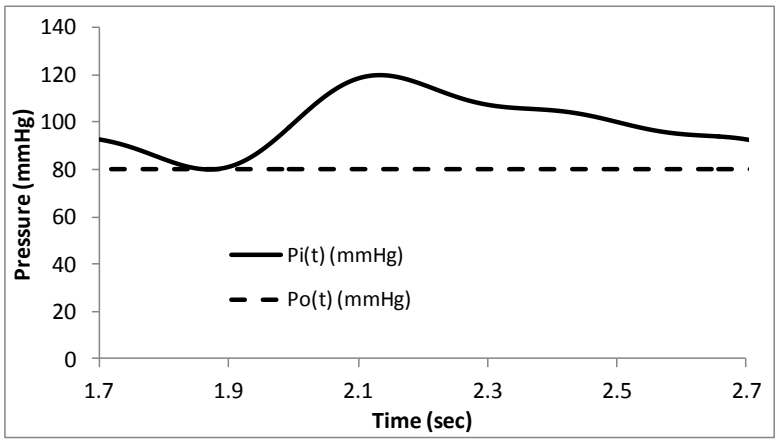

(a)

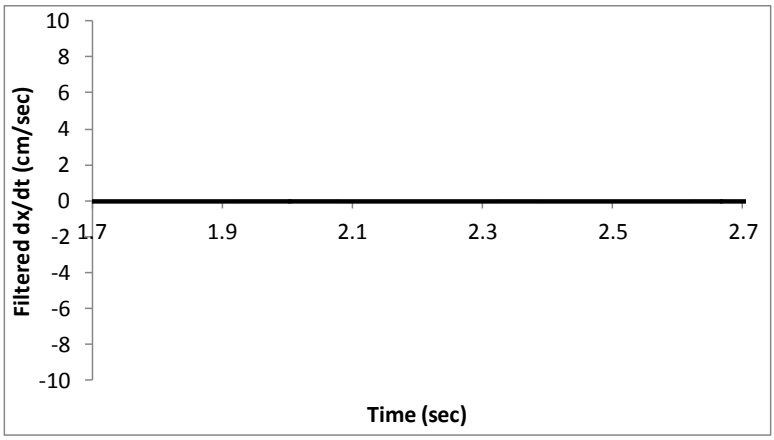

(b)

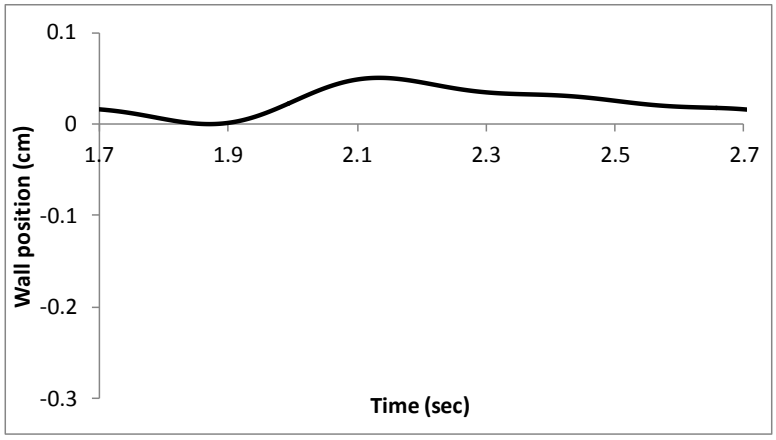

(c)

Figure 12. Simulated wall motion with cuff pressure at 80 mmHg equal to true diastolic pressure. There are no sounds (b). Details similar to Figure 5.

The forgoing simulations raise the question of what might happen near diastolic blood pressure if the transition between expanded state and the collapsed, or buckled, state occurred a level $x < 0$, for example $x = -0.03\ r_0$. In this case buckling begins at a threshold negative displacement somewhat less than the zero pressure radius, as suggested by the work of Cohen and Dinar[35] on elastic tubes. Figure 13 compares time domain records of wall position for state transition at $x^* = 0$ versus state transition at $x^* = -0.03 r_0$. If radial contraction without buckling is allowed at small negative transmural pressures, such as occur during cuff deflation just before the diastolic end point, there is no state transition and no sound. This effect pushes the disappearance of arterial sounds higher than true diastolic pressure.

The phenomenon indicated in Figure 13 suggests that, if anything, the point of disappearance of arterial sounds may slightly overestimate true diastolic pressure. Since buckling is unlikely to begin exactly at the zero pressure artery radius ($x^* = 0$) but rather at a point slightly below it ($x^* < 0$), the disappearance of arterial sounds will occur at a cuff pressure slightly above true diastolic pressure, on average, depending on how the beats fall in the time domain. This observation strengthens the choice of the point of disappearance of the sounds, rather than muffling, as the better endpoint, and may help resolve the diastolic dilemma.

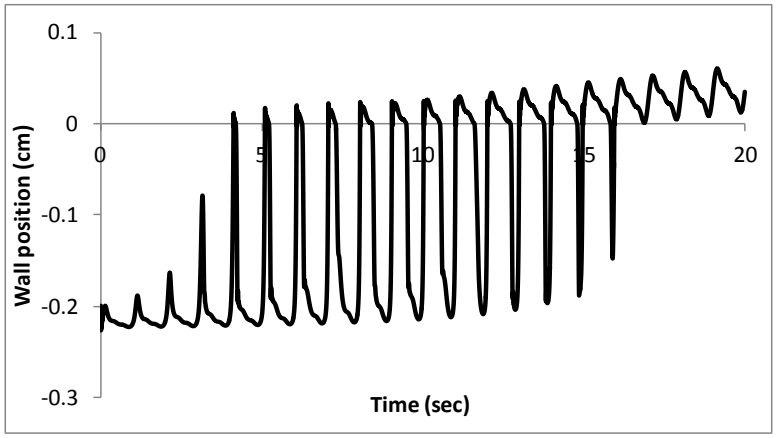

(a)

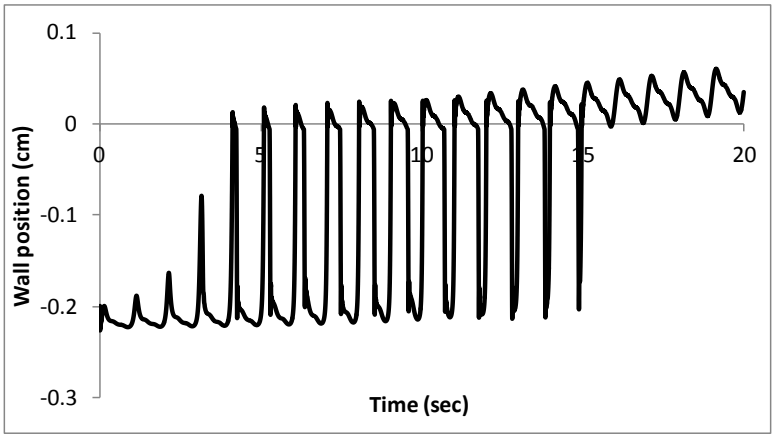

(b)

Figure 13. Wall position versus time during cuff deflation with buckling beginning at $x^* = 0$ (a) and buckling beginning at $x^* = -0.03r_0$ (b). Large swings in wall motion cease one heartbeat earlier at t = 15 sec in the case of delayed buckling, causing an over-estimate of diastolic pressure.

Critical role of state transition

The role of state transition in generating arterial sounds can be explored by simulating varying degrees of mismatch between wall stiffness during buckling vs. wall stiffness during expansion. Figure 14(a) shows a simulation in which there is no discontinuity between collapse and expansion phases. (This condition was created by setting $x^* << -r_0$.) In this case there are no audible sounds. The record of wall motion shows a smooth following of the arterial pressure waveform. As the degree of mismatch is increased by decreasing collapse phase stiffness, sounds appear and get louder. Figures 14(b) shows high pass filtered sounds, labeled filtered dx/dt, during cuff deflation for collapse phase arterial stiffnesses 10 times the nominal value, but still less than expansion phase stiffness. This case represents a smaller than normal mismatch in stiffness. Figure 14(c) shows sounds for collapse phase stiffness one half the nominal value, or about $1/20^{th}$ expansion phase stiffness. This case represents a larger than normal mismatch is

stiffness. Sound intensity increases as collapse phase stiffness becomes smaller with respect to expansion phase stiffness. Also splitting of the sounds becomes more prominent, since sudden deceleration in late buckling begins to occur, owing to the nonlinear increase in stiffness as buckling proceeds toward complete flattening. These effects support the hypothesis that it is sudden deceleration of wall motion, either in expansion or in flattening, that produces arterial sounds.

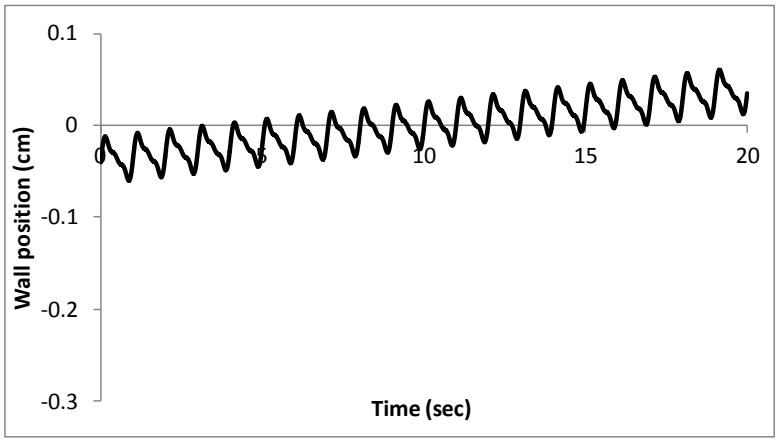

(a)

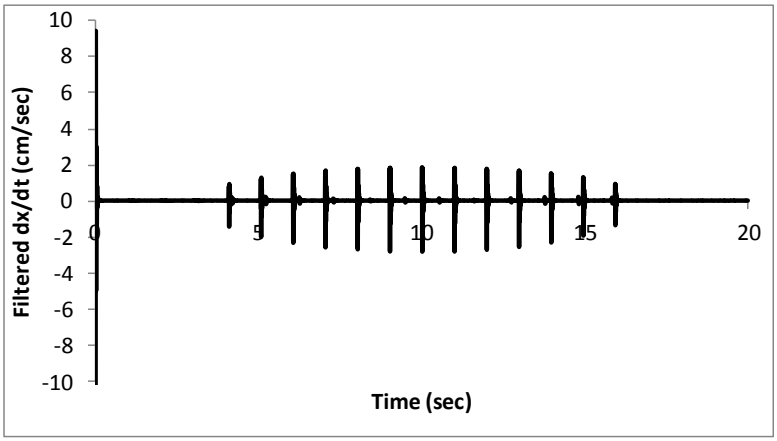

(b)

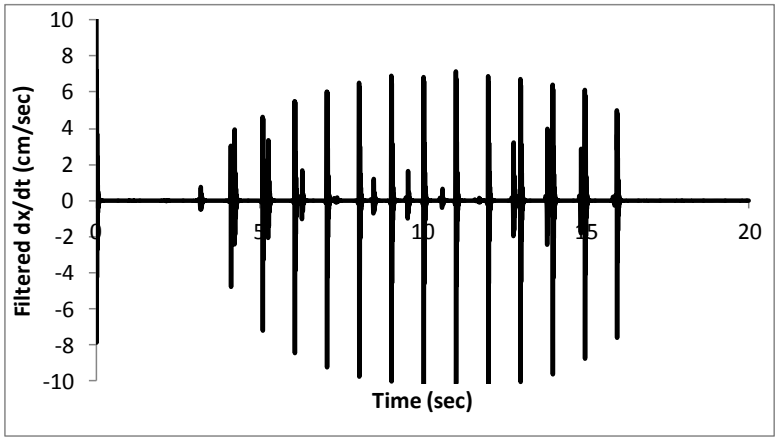

(c)

Figure 14. Effects of changing collapse phase stiffness. (a) Wall motion with collapse phase stiffness equal to expansion phase stiffness. There are no sounds. (b) High pass filtered sounds with collapse phase stiffness ten times the nominal value, but still less than expansion phase stiffness. (c) High pass filtered sounds with collapse phase stiffness half the nominal value, and substantially less than expansion phase stiffness. Greater mismatch in stiffness between collapse and expansion phases results in louder simulated arterial sounds.

Narrowing of the mismatch between collapse phase and expansion phase stiffness can be regarded as the cause of muffling associated with venous congestion in the limb that is being used for the measurement. As blood accumulates in the arteries, capillaries, and veins downstream of the cuff, it cannot drain back to the heart via brachial and cephalic veins because of total venous occlusion by the cuff. The resulting back pressure makes it more difficult for the artery segment beneath the cuff to collapse, splinting the artery and increasing the effective k_2. The increased effective k_2 attenuates the amplitude of the Korotkoff sounds, as just demonstrated, accounting for muffling. This idea is also supported by the practical observations of the author and his mentor, L.A. Geddes, that muffling can be reduced by raising he arm prior to cuff inflation to drain venous blood from downstream vessels, by initially inflating the cuff as rapidly as possible, and by deflating the cuff more quickly between the systolic and diastolic end points to minimize accumulation of blood distal to the cuff during the measurement.

Other effects of changing parameters

The present one dimensional model of arterial wall mechanics allows exploration of other variables influencing arterial sound generation (data not shown). In summary, increasing pulse pressure, as in exercise, increases the amplitude of the arterial sounds, and low pulse pressure, as in heart failure or subclavian stenosis, decreases the amplitude of the arterial sounds. Larger scale arteries, characterized by larger r_0 and h_0, in adults produce increased arterial sound amplitude, and smaller arteries in children produce decreased arterial sound amplitude. Increasing artery wall stiffness, as in older individuals, increases arterial sound frequency. Decreasing artery wall stiffness, as in younger individuals, decreases arterial sound frequency. Similarly, increasing effective mass, as in obesity, decreases arterial sound frequency and *vis versa*.

Audio playback of simulated arterial sounds

As a final subjective validation of the one dimensional model of artery wall motion, the computed arterial sounds were converted to .wav files using open source software written by Axel Brink, 21-May-2002 (www.freevbcode.com) and played on a harman/kardon (Northridge, CA) Model HK695 subwoffer multimedia speaker, having a frequency response of 35 Hz – 20,000Hz. Unlike standard speakers for desktop or laptop computers, the harman/kardon speaker is able to reproduce deep bass tones characteristic of the arterial sounds. The experiment was highly successful in that the playback of simulated arterial sounds sounded very much like real Korotkoff sounds heard with a stethoscope over the brachial arteries of normal human subjects.

Discussion

In the early to mid-twentieth century Korns[36] and Groedel and Miller[37] published rare high speed time-domain tracings of Korotkoff sounds from normal human adults that clearly show transient damped sinusoidal waves. These actual sounds can be compared to modeled sounds as a point of validation. As shown, for example, in Figure 9, the frequencies of model Korotkoff sounds for a normal case were about 72 Hz. The frequencies of real human Korotkoff sounds recorded by Korns and by Groedel and Miller ranged from 60 to 80 Hz. Also the durations of typical model transients averaged 90 milliseconds. The durations measured by Korns and by Groedel and Miller for human Korotkoff sounds ranged from 70 to 100 milliseconds. If one examines at the published waveforms recorded from human subjects on an expanded time scale, they closely resemble the model results. That is, the shapes or envelopes of simulated and real Korotkoff sounds are the same. Hence the frequencies, durations, and shapes of simulated waveforms match those of actual Korotkoff sounds, validating the one-dimensional spring-mass-damper model of Figure 3.

Such transient resonances are well explained by the physics of wall motion alone. In particular, the sudden deceleration of the expanding arterial wall as it transitions from the buckled state to the expanding state causes ringing at a natural resonant frequency determined by the elasticity and dimensions of the artery wall and the mass of outward moving tissue. The stiffness of spring k_1 must be substantially greater than that of spring k_2 to provide such abrupt deceleration of the arterial wall at the beginning of the expansion phase. This condition is met because wall stretching in expansion requires fundamentally more force than wall bending in buckling. There will be only one Korotkoff sound per heartbeat if spring k_2 is stiff enough and appropriately nonlinear so as to gradually decelerate the collapsing artery wall during buckling. In some situations a second sound occurs with each pulse during the collapse phase if there is abrupt deceleration prior to wall-to-wall contact.

The present mathematical model of artery wall motion during cuff deflation also sheds light on the diastolic dilemma and the practical choice of an end point for determination of diastolic pressure. If cuff pressure is completely transferred to the outside wall of the artery, and if buckling begins at radius $r = r_0$, then the disappearance of Korotkoff sounds corresponds exactly to diastolic pressure. If cuff pressure is inefficiently transferred to the outside of the artery or if buckling begins at a radius $r < r_0$, then the disappearance of Korotkoff sounds will occur at a cuff pressure slightly above true diastolic arterial pressure. Any sounds that occur after this diastolic end point should have different frequency characteristics, perhaps being caused by blood flow rather than wall motion. In this case it should be possible to design physical or electronic filters to distinguish them and make the diastolic end point more accurate in clinical practice.

Alternative theories

Many alternative hypotheses have been proposed for the generation of Korotkoff sounds, including including the water hammer mechanism, in which the jet of blood released upon opening of the lumen of the artery collides with static downstream blood to produce a shock

wave; the pistol shot mechanism, in which the rapid motion of the arterial wall causes downstream turbulent blood flow; turbulent blood flow through a partially collapsed and restricted artery segment; shock waves induced by the leading edge of the blood pressure pulse; cavitation; and, as in the present paper, phenomena related to buckling and unbuckling of the arterial wall[4, 6, 39-41]. The various concepts regarding the genesis of Korotkoff sounds can be classified into two main categories: fluid turbulence and oscillations of the arterial wall beneath or distal to the cuff. The strengths and weaknesses of various competing theories have been well discussed previously[4, 40].

Notably, the experiments of McCutcheon and Rushmer[31], using dual Doppler ultrasound to track both arterial wall motion and blood flow, demonstrated that the Korotkoff sounds and wall velocity spikes were coincident in time and terminated long before peak blood flow velocity was attained. Also, recorded oscillations in blood flow velocity, perhaps representing turbulence, persisted long after the end of the Korotkoff sounds. Moreover, the ultrasonically measured blood flow velocity patterns "displayed no consistent recognizable change in form as cuff pressure passed through the level of diastolic pressure, except under conditions of extreme vasodilation (i.e., reactive hyperemia)."

After their extensive experimental studies McCutcheon and Rushmer[31] concluded that the initial high frequency component of the Korotkoff sound "occurs at the very onset of flow under the cuff and probably represents an acceleration transient producing abrupt displacement of the arterial wall and surrounding tissues distal to the point of compression". They further concluded that the appearance and disappearance of the "initial transient sound", which "contains frequencies in the range between 60 and 180 cycle/sec" constitutes the criterion for determining both systolic and diastolic pressures. The present biomechanical investigation comes to essentially the same conclusion.

Nonetheless, studies and discussion of blood flow and turbulence as contributers to the genesis of Korotkoff remain prominent in the literature. For example Chungcharoen[42] studied sounds produced when a small rubber cuff, about one centimeter wide, was placed loosly around a surgically isolated carotid artery in anesthetized dogs and found that weaker, Korotkoff-like sounds could still be detected when an arterial segment was replaced by a constricted glass tube, suggesting that wall motion could not be their origin. The waveform and frequency of sounds downstream of the glass tube were similar to those recorded with a natural artery. However, the very narrow cuff used in this study may well have produced turbulent flow by virtue of creating a local stenosis, rather than mimicing the mechanics of the human arm and external cuff.

Drzewiecki, Melbin, and Noordergraaf[40] conducted perhaps the most extensive modern investigation into possible flow-related mechanisms for generation of Korotkoff sounds. They employed an electrical analogy and equivalent circuit to formulate the governing state equaitons for fluid dynamic components and the nonlinear lumped compliance of a collapsible artery segment. There were five collapsible vessel parameters, adjusted by method of nonlinear least-squares estimation to minimize a chi-square figure of merit. The model Korotkoff sound was derived from the distal pulse pressure and high pass filtered to determine sound content. The frequency of the sound was in the range of 5 to 10 Hz with maximal power less than 20 Hz in most cases. Individual computed sounds consisted of one or two cycles per heartbeat. The

envelope of the computed Korotkoff sound amplitude during cuff deflation resembled a descending ramp, which is not typical for recorded Korotkoff sounds in man. This detailed simulation study showed that flow pulses can contain sub-audible sonic information under realistic conditons. However, the sound is near 10 Hz, below the typical human threshold for hearing, and not near 70 Hz as demonstrated in vivo by high speed recordings[36, 37]. This study may well have correctly rendered the low frequency and largely inaudible components of arterial sounds, but may it have missed the source of the higher frequency, sharper sounds that are used clinically to measure blood pressure by the ausculatatory method.

Audible vs. inaudible frequencies

Because of the design and function of the human cochlea, humans are not able to hear tones below 20 Hz [43]. The accepted value for the frequency range of human hearing is 20 to 20,000 Hz.[44] Both the frequency transmission of the stethoscope[17] and the sensitivity of the human ear drop off dramatically at low frequencies approaching 20 Hz and below. The difference in each case is about 20 dB or 10-fold in sound pressure between 100 and 20 Hz. Most likely it is the high frequency components of the Korotokoff sounds, namely the "K_1" components caused by wall resonance, at frequencies of 50 Hz and above that are heard in clinical practice. Lower frequency sounds in the neighborhood of 10 Hz that are associated with other propossed mechanisms such as blood acceleration or the water hammer effect are simply not heard.

Conclusions

The simple act of measuring blood pressure with a cuff and stethoscope by the auscultatory method can have profound implications for a patient[2]. A falsely high reading can lead to costly diagnostic studies or possible life-long drug therapy. Further, since the auscultatory method is used to evaluate the accuracy of automatic blood pressure devices[45-47], there can be propagation of errors across technologies. Although the accuracy of cuff-based measurements is often taken for granted, many subtle factors can cause clinically significant errors, including: cuff size, cuff deflation rate, the starting point for cuff deflation, psychological factors, arm elevation and tension, the presence of atrial fibrillation, the observer's terminal digit preference (even 5's or 0'), the type of manometer, and the frequency response of the stethoscope or recording microphone[34, 35]. Included also in this list is the choice of endpoint and especially the diastolic dilemma.

By offering a simple mechanical explanation for the origin of the audible Korotkoff sounds, the wall resonance hypothesis provides a biophysical solution to the diastolic dilemma, helping to resolve a longstanding debate about one of the most basic aspects of clinical care. Better theoretical understanding of wall resonance also suggests the possibility of creating special purpose mechanical stethoscopes or electronic filters for use in blood pressure determinations that would even better separate the higher frequency tones of arterial resonance, from the lower frequency and/or broadband sounds of turbulent blood flow. Such technologies could objectively resolve in a quantitative way the difference between muffling and disappearance of the Korotkoff sounds, providing a more accurate end point for true diastolic pressure. By

example, the present research also demonstrates how mathematical modeling can be used as a tool for discovery as well as for research synthesis.

Appendix 1: force vs. displacement and spring constant during expansion

Figure 15 shows a diagram of a thin walled cylindrical elastic tube of inner radius, r, wall thickness, h, and length, L, subjected to internal pressure, P_i, and external pressure P_o, with transmural pressure $\Delta P = (P_i - P_o)$. The zero pressure internal radius is r_0 and the zero pressure wall thickness is h_0. A sector of the tube, $\Delta\theta$, is shown. The normal force, ΔF, on the sector created by the transmural pressure difference is $\Delta F = \Delta P\, Lr\Delta\theta$. The pressure induces stress, σ, in the tube wall in the hoop dimension. By deduction from Figure 15 the opposite directed reactive force from elastic stretch of the segment is $\Delta F_R = \sigma hL \cdot 2\sin(\Delta\theta/2)$.

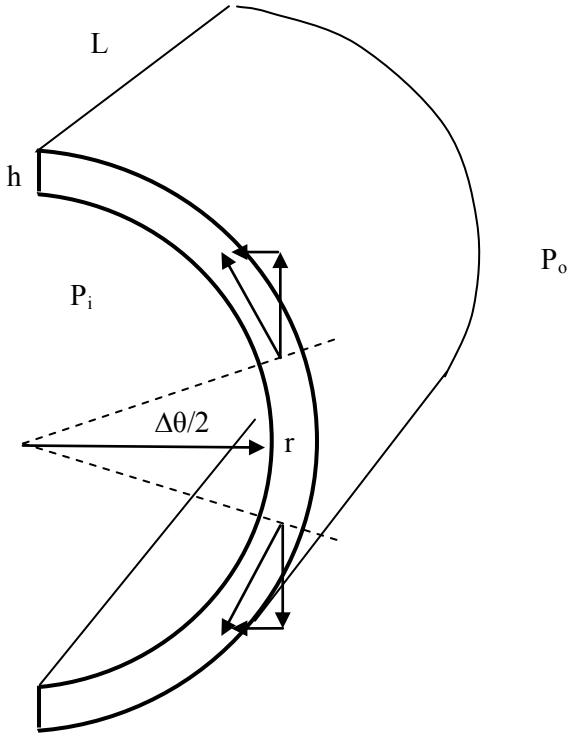

Figure 15. Diagram of thin walled elastic tube. Arrows indicate forces on ends of segment $r_0\Delta\theta$, resolved into components parallel and normal to radius r.

As in the main body text, let $x = \Delta r$, the change in radius during expansion. Then Young's modulus of the wall material is $E = \sigma/(x/r_0)$, that is, stress divided by strain, and in turn

$$\Delta F_R = \frac{Ex}{r_0} hL \cdot 2\sin(\Delta\theta/2). \tag{14}$$

Using $\sin(u) \approx u$ for small angles, u, in radians

$$\Delta F_R \approx \frac{Ex}{r_0} hL \cdot \Delta\theta. \tag{15}$$

The spring constant, k_1, during expansion is $\Delta F_R/x$ or

$$k_1 \approx \frac{EhL}{r_0} \Delta\theta. \tag{16}$$

For small positive Δr in an artery with typical nonlinear characteristics of a biomaterial, E will increase and h will decrease as x increases, producing offsetting errors, so that

$$k_1 \approx \frac{Eh_0L}{r_0} \Delta\theta, \tag{17}$$

which is constant.

Appendix 2: force vs. displacement and spring coefficient during buckling

Figure 16 shows the strained shape adopted by the cross-section of one half of a fully flattened elastic tube. The zero pressure internal radius is r_0 and the zero pressure wall thickness is h_0. The length of the half segment perpendicular to the page is L. The fully flattened shape can be closely approximated by a rectangle of height $2h_0$ capped by a semicircle of radius h_0. Young's modulus of the wall material is denoted E. The spring coefficient, k_2, for wall displacement $x = -r_0$ can be approximated as the force required for complete flattening, divided by the absolute value of the distance, r_0, moved by the inner wall of the tube orthogonal to the plane of flattening, as follows.

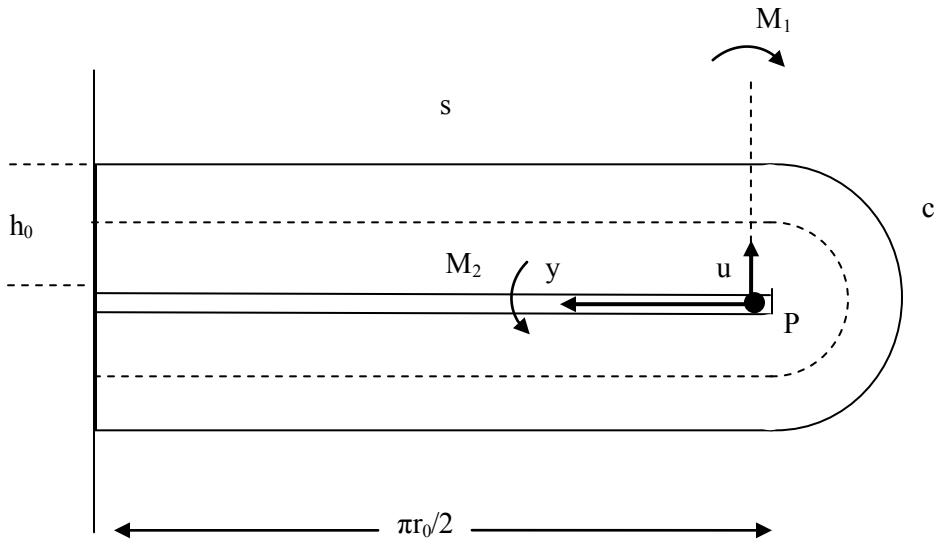

Figure 16. Sketch of one half of completely flattened elastic tube. Bending moments, M_1 and M_2 are indicated by curved arrows.

In Figure 16 the dashed line represents a curved surface at uniform distance, u, from the inner wall of the compressed tube. The circular path length at u before bending is $p = \pi(r_0 + u)$. The path length at u after complete flattening is $2\left(\frac{\pi r_0}{2}\right) + \pi u = \pi(r_0 + u) = p$. Hence, there is no stretching; only bending of the wall material.

The force required to produce maximal bending can be calculated as follows. Consider bending moment M_1 about point P. Compression of the outer regions of straight segment, s, adds to bending moment M_1. Also stretching of curved segment, c, further adds to bending moment M_1. Let $\phi = \frac{\pi r_0}{\pi(r_0 + u)} = \frac{1}{1 + u/r_0}$ be the fractional path at level u that is straight. Length ϕp is shortened or compressed by factor $\frac{u}{r_0 + u} = 1 - \phi$; the absolute compression at level u is $\phi p(1-\phi)$. At the same time length $(1-\phi)p$ is stretched by amount $\phi p(1-\phi)$, also adding to bending moment M_1, by virtue of the continuity of the straight and curved segments. Noting that the spring constant in compression or stretching of a rectangular volume of elastic material having Young's modulus, E, is E·area/length, the combined compression and stretching will produce an incremental bending moment

$$dM_1 = \phi(1-\phi)p\left[\frac{ELdu}{\phi p}\right]u + \phi(1-\phi)p\left[\frac{ELdu}{(1-\phi)p}\right]u, \text{ or} \qquad (18)$$

$$dM_1 = (1-\phi)ELu\,du + \phi ELu\,du = ELu\,du\,. \tag{19}$$

In turn,

$$M_1 = \int dM_1 = EL\int_0^{h_0} u\,du = \frac{1}{2}ELh_0^2\,. \tag{20}$$

The incremental counterbalancing bending moment, dM_2, created by external pressure acting on straight segment, s, at distance y from point, P, in Figure 16 is $dM_2 = \Delta P(L\cdot dy)y$, and

$$M_2 = \int dM_2 = \Delta PL\int_0^{\pi r_0/2} y\,dy = \Delta P\cdot L\frac{1}{2}\cdot\frac{\pi^2 r_0^2}{4}\,. \tag{21}$$

Setting $M_1 = M_2$ gives

$$\Delta P = \frac{4E}{\pi^2}\cdot\frac{h_0^2}{r_0^2}\,. \tag{22a}$$

As a reality check suppose E = 1.4 x 10^6 dynes/cm^2 and $h_0/r_0 = 0.15$, as in the standard model. Then the collapse pressure for an artery would be

$$\Delta P = \frac{4\cdot 1.4\cdot 10^6 E}{(3.14)^2}\cdot(0.15)^2\,\frac{\text{dynes}}{\text{cm}^2}\cdot\frac{1\,\text{mmHg}}{1333\,\text{dynes/cm}^2} = 9.6\ \text{mmHg}\,, \tag{22b}$$

or about 10 mmHg outside greater than inside, which is physically reasonable and consistent with overpressures required to suppress cuff pressure oscillations[4].

Now consider the small sector of the collapsed tube of surface area, $r_0\Delta\theta L$, perpendicular to the plane of flattening. The reactive elastic force in buckling on this sector is

$$\Delta F_R = \Delta P\cdot r_0\Delta\theta L = \frac{4E}{\pi^2}\cdot\frac{h_0^2}{r_0^2}\cdot r_0\Delta\theta L\,, \tag{23}$$

and the effective, positive signed, spring "constant" or coefficient at $x = -r_0$ is $\Delta F_R/r_0$, or

$$k_2(-r_0) = \frac{4EL}{\pi^2}\cdot\frac{h_0^2}{r_0^2}\Delta\theta\,. \tag{24}$$

Appendix 3: effective mass

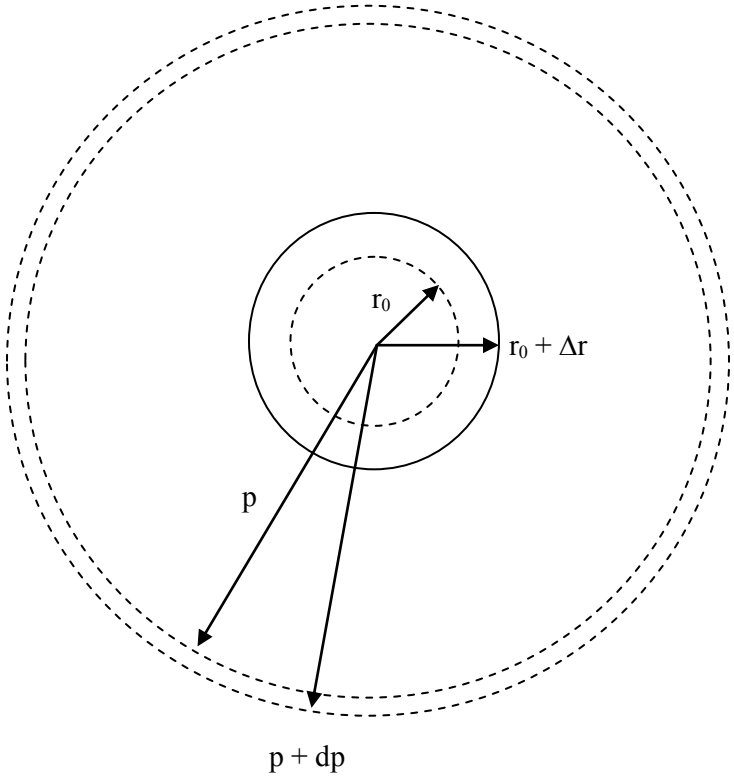

Figure 17. Expanding cylindrical shell of incompressible fluid.

Figure 17 shows a cross section of the inner wall of an expanding cylindrical elastic tube having zero pressure radius r_0, and time varying radius $r = r_0 + \Delta r$. As the tube expands it pushes surrounding fluid outward, and as it contracts it draws surrounding fluid inward. Consider a shell of incompressible fluid at radius, p, having thickness dp and containing fluid of density, ρ. Let u represent the velocity of radial movement of the fluid in the shell at radius, p. For an incompressible fluid, we must have

$$\rho \cdot 2\pi rL \cdot \frac{dr}{dt} = \rho \cdot 2\pi pL \cdot u \,, \qquad (25)$$

which gives $u = \frac{r}{p}\frac{dr}{dt}$. At increasingly farther radii, p, the outward movement of fluid becomes slower. For the small displacement case $r \approx r_0$ the acceleration of the cylindrical shell at radius p is

$$\frac{du}{dt} \approx \frac{r_0}{p} \cdot \frac{d^2r}{dt^2}. \tag{26}$$

This simplification allows straightforward calculation of the resonant frequency of the system by means of an analytical formula for an ordinary second order differential equation.

For concentric shells of constant thickness, dp, the incremental "mass x acceleration" of the shell is

$$\rho 2\pi pL\,dp\,\frac{du}{dt} \approx \rho 2\pi pL\,dp \cdot \frac{r_0}{p} \cdot \frac{d^2r}{dt^2}. \tag{27}$$

The total "mass x acceleration" of all shells added together from radius 0 to the outer radius of tissue, R_{max}, surrounding the artery is

$$\text{"ma"} \approx 2\pi\rho L r_0 \cdot \frac{d^2r}{dt^2}\int_0^{R_{max}} dp = 2\pi\rho L r_0 \cdot \frac{d^2r}{dt^2} R_{max}. \tag{28}$$

Since, as defined in the body text, the acceleration of the artery wall model, $\frac{d^2r}{dt^2} = \ddot{x}$; the effective mass of the system is

$$m \approx 2\pi\rho L r_0 R_{max}. \tag{9}$$

For a sector of the tube having angle, $\Delta\theta$, the effective mass is

$$m \approx \Delta\theta\rho L r_0 R_{max}. \tag{30}$$

(For larger excursions in which r becomes much greater than r_0, the corresponding expression for "mass x acceleration" (derivation not shown) is

$$\text{"ma"} = \Delta\theta\left(\rho L(r_0 + x)R_{max}\,\ddot{x} + \rho L R_{max}\,\dot{x}^2\right), \tag{31}$$

which can be substituted into an equation of motion that can be solved numerically. However, for the present problem of artery wall motion the simpler solution assuming that r is close to r_0 is sufficient, since the stiffness of the artery in expansion is much greater than the stiffness in

buckling and also since the transmural wall pressures during an auscultatory reading are relatively small.)

Acknowledgements

None

References

1. Geddes LA, Moore AG. The efficient detection of korotkoff sounds. *Medical & biological engineering*. 1968;6:603-609
2. O'Brien E, Asmar R, Beilin L, Imai Y, Mallion JM, Mancia G, Mengden T, Myers M, Padfield P, Palatini P, Parati G, Pickering T, Redon J, Staessen J, Stergiou G, Verdecchia P. European society of hypertension recommendations for conventional, ambulatory and home blood pressure measurement. *Journal of hypertension*. 2003;21:821-848
3. O'Brien ET, O'Malley K. Abc of blood pressure measurement: Technique. *Br Med J*. 1979;2:982-984
4. Geddes LA. *The direct and indirect measurement of blood pressure*. Chicago: Year Book Medical Publishers, Inc.; 1970.
5. Geddes LA, Hoff HE. Introduction of the auscultatory method of measuring blood pressure--including a translation of korotkoff's original paper. *Cardiovascular Research Center Bulletin*. 1966;5:57-73
6. Venet R, Miric D, Pavie A, Lacheheb D. Korotkoff sound: The cavitation hypothesis. *Medical hypotheses*. 2000;55:141-146
7. Burton AC. The criterion for diastolic pressure--revolution and counterrevolution. *Circulation*. 1967;36:805-809
8. Voors AW, Webber LS, Berenson GS. A choice of diastolic korotkoff phases in mercury sphygmomanometry of children. *Preventive medicine*. 1979;8:492-499
9. Shennan A, Gupta M, Halligan A, Taylor DJ, de Swiet M. Lack of reproducibility in pregnancy of korotkoff phase iv as measured by mercury sphygmomanometry. *Lancet*. 1996;347:139-142
10. De Mey C. Method specificity of the auscultatory estimates of the inodilatory reduction of diastolic blood pressure based on korotkoff iv and v criteria. *British journal of clinical pharmacology*. 1995;39:485-490
11. Juel A, Heap A. The reopening of a collapsed fluid-filled elastic tube. *Journal of Fluid Mechanics*. 2007;572:287-310
12. Bertram CD. The effects of wall thickness, axial strain and end proximity on the pressure-area relation of collapsible tubes. *J Biomech*. 1987;20:863-876
13. Kresch E. Compliance of flexible tubes. *J Biomech*. 1979;12:825-839
14. Kozlovsky P, Zaretsky U, Jaffa AJ, Elad D. General tube law for collapsible thin and thick-wall tubes. *J Biomech*. 2014;47:2378-2384
15. Bassez S, Flaud P, Chauveau M. Modeling of the deformation of flexible tubes using a single law: Application to veins of the lower limb in man. *J Biomech Eng*. 2001;123:58-65
16. Drzewiecki G, Field S, Moubarak I, Li JK. Vessel growth and collapsible pressure-area relationship. *Am J Physiol*. 1997;273:H2030-2043
17. Yu C, Tsai TH, Huang SI, Lin CW. Soft stethoscope for detecting asthma wheeze in young children. *Sensors (Basel)*. 2013;13:7399-7413

18. Holzapfel GA, Ogden RW. Modelling the layer-specific three-dimensional residual stresses in arteries, with an application to the human aorta. *Journal of the Royal Society, Interface / the Royal Society*. 2010;7:787-799
19. Fung YC. *Biomechanics: Mechanical properties of living tissues*. New York: Springer-Verlag; 1981.
20. Bank AJ, Kaiser DR, Rajala S, Cheng A. In vivo human brachial artery elastic mechanics: Effects of smooth muscle relaxation. *Circulation*. 1999;100:41-47
21. Cox RH. A model for the dynamic mechanical properties of arteries. *J Biomech*. 1972;5:135-152
22. Gow BS, Taylor MG. Measurement of viscoelastic properties of arteries in the living dog. *Circ Res*. 1968;23:111-122
23. Bergel DH. The visco-elastic properties of the arterial wall. 1960;Ph.D.:250
24. Lawton RW. Measurements on the elasticity and damping of isolated aortic strips of the dog. *Circ Res*. 1955;3:403-408
25. Learoyd BM, Taylor MG. Alterations with age in the viscoelastic properties of human arterial walls. *Circ Res*. 1966;18:278-292
26. Betik AC, Luckham VB, Hughson RL. Flow-mediated dilation in human brachial artery after different circulatory occlusion conditions. *American journal of physiology. Heart and circulatory physiology*. 2004;286:H442-448
27. Iwamoto Y, Maruhashi T, Fujii Y, Idei N, Fujimura N, Mikami S, Kajikawa M, Matsumoto T, Kihara Y, Chayama K, Noma K, Nakashima A, Higashi Y. Intima-media thickness of brachial artery, vascular function, and cardiovascular risk factors. *Arteriosclerosis, thrombosis, and vascular biology*. 2012;32:2295-2303
28. Weidinger F, Frick M, Alber HF, Ulmer H, Schwarzacher SP, Pachinger O. Association of wall thickness of the brachial artery measured with high-resolution ultrasound with risk factors and coronary artery disease. *Am J Cardiol*. 2002;89:1025-1029
29. Suessenbacher A, Dorler J, Wunder J, Hohenwarter F, Alber HF, Pachinger O, Frick M. Comparison of brachial artery wall thickness versus endothelial function to predict late cardiovascular events in patients undergoing elective coronary angiography. *Am J Cardiol*. 2013;111:671-675
30. Wijnhoven HA, de Boer MR, van Maanen MJ, van Dongen DM, Kraaij SF, Smit T, Visser M. Reproducibility of measurements of mid-upper arm circumference in older persons. *Journal of human nutrition and dietetics : the official journal of the British Dietetic Association*. 2013;26:24-31
31. McCutcheon EP, Rushmer RF. Korotkoff sounds. An experimental critique. *Circ Res*. 1967;20:149-161
32. Boron WF, Boulpaep EL. *Medical physiology*. Philadelphia: Elsevier; 2005.
33. Geddes LA, Baker LE. *Prinicples of applied biomedical instrumentation, second edition*. 1975.
34. Geddes LA, Spencer WA, Hoff HE. Graphic recording of the korotkoff sounds. *American heart journal*. 1959;57:361-370
35. Cohen D, Dinnar U. Buckling of fluid-filled elastic cylindrical tubes under dynamic pressure. *Israel Journal of Technology*. 1975;13:192-201
36. Korns HM. The nature and time relations of the compression sounds of korotkoff in man. *American Journal of Physiology*. 1926;76:247-264
37. Groedel F, Miller M. Graphic study of auscultatory blood pressure measurement. *Experimental Medicine and Surgery*. 1943;1:148-162
38. Bertram CD, Pedley TJ. A mathematical model of unsteady collapsible tube behaviour. *J Biomech*. 1982;15:39-50
39. Ur A, Gordon M. Origin of korotkoff sounds. *Am J Physiol*. 1970;218:524-529
40. Drzewiecki GM, Melbin J, Noordergraaf A. The korotkoff sound. *Ann Biomed Eng*. 1989;17:325-359

41. Conrad WA, McQueen DM, Yellin EL. Steady pressure flow relations in compressed arteries: Possible origin of korotkoff sounds. *Med Biol Eng Comput*. 1980;18:419-426
42. Chungcharoen D. Genesis of korotkoff sounds. *Am J Physiol*. 1964;207:190-194
43. Bekesy Gv. The vibration of the cochlear partition in anatomical preparations and in models of the inner ear. *The Journal of the Acoustical Society of America*. 1949;21:233-245
44. D'Ambrose C. Frequency range of human hearing: The physics factbook. 2003
45. Graettinger WF, Lipson JL, Cheung DG, Weber MA. Validation of portable noninvasive blood pressure monitoring devices: Comparisons with intra-arterial and sphygmomanometer measurements. *American heart journal*. 1988;116:1155-1160
46. White WB, Anwar YA. Evaluation of the overall efficacy of the omron office digital blood pressure hem-907 monitor in adults. *Blood pressure monitoring*. 2001;6:107-110
47. El Assaad MA, Topouchian JA, Asmar RG. Evaluation of two devices for self-measurement of blood pressure according to the international protocol: The omron m5-i and the omron 705it. *Blood pressure monitoring*. 2003;8:127-133